From Department of Pharmacology and Physiology
Karolinska Institutet, Stockholm, Sweden

ENGINEERING CELL COMMUNICATION FROM NANOSCALE TO TISSUE LEVELS TOWARDS THERAPEUTIC APPLICATIONS

Christina Kolonelou

Karolinska Institutet

Stockholm 2024

Published by Karolinska Institutet.
Printed by Universitetsservice US-AB, 2024

ISBN 978-91-8017-269-1

Engineering cell communication from nanoscale to tissue levels towards therapeutic applications
Thesis for Doctoral Degree (Ph.D.)

By

Christina Kolonelou

The thesis will be defended in public at Peter Reichard, Biomedicum, Solnavägen 9, Solna, Stockholm, on Friday March 22nd, 2024, at 09:30

Principal Supervisor:
Ana Teixeira
Karolinska Institutet
Department of Physiology and Pharmacology
Division of Nanomedicine and Spatial Biology

Co-supervisor(s):
Björn Högberg
Karolinska Institutet
Department of Medical Biochemistry and Biophysics
Division of Medical Systems Bioengineering

Ernest Arenas
Karolinska Institutet
Department of Medical Biochemistry and Biophysics
Division of Molecular Neurobiology

Olov Andersson
Karolinska Institutet
Department of Cell and Molecular Biology

Opponent:
Maartje M.C. Bastings
Swiss Federal Institute of Technology in Lausanne (EPFL)
Department of Interfaculty Bioengineering Institute

Examination Board:
Kaska Koltowska
Uppsala University
Department of Immunology, Genetics and Pathology
Division of Vascular Biology

Samir El Andaloussi
Karolinska Institutet
Department of Laboratory Medicine
Division of Biomolecular and Cellular Medicine

Erdinc Segzin
Karolinska Institutet
Department of Women's and Children's Health
Division of Clinical Paediatrics

To all those who believed in me

“Your world is as big as you make it.”
Georgia Douglas Johnson

POPULAR SCIENCE SUMMARY OF THE THESIS

Cells in multicellular organisms do not live in isolation; instead, they engage in social behavior by constantly communicating with each other and their environment through messenger molecules. In this world of our body's tiny messengers, hiccups in communication often spark health issues. Figuring out the complex ways these biological signals work is key to crafting smart solutions for effective disease treatments.

In this thesis, we combined cell biology, novel tools and the small tropical fish called zebrafish to study cell communication and contribute to the development of novel therapeutic strategies.

In the first part of this work (Paper I), we used a small device, acting as miniaturized laboratory, to artificially create neuromuscular junctions-a vital communication hub in the body that controls our movement- and identify messenger molecules exchanged between nerves and muscles.

In the following parts (Papers II, III and IV) we employed a technique known as DNA origami, where DNA is folded and shaped into precise structures- as origami with paper but on a molecular level. This innovative approach provides us with the ability to manipulate DNA and engineer minuscule architectures, almost like using a toolkit at the nanoscale. DNA nanostructures can act as customizable couriers, delivering molecular messages to their designated molecules on the cell membrane- the receptors- with precision. These interactions can potentially influence cellular behavior. In paper II we were able tweak how the messenger molecule insulin interacts with its receptors, by arranging insulin molecules into well-defined groups on the surface of DNA nanostructures. In Paper III, we investigated how DNA nanostructures that emit light when exposed to specific wavelengths, interact with tissues and cells in a living organism. Here zebrafish in their early stages of life served as the animal model, leveraging their transparency to enable the observation of these interactions. Lastly, in paper IV we suggest a method that can help to check how well DNA nanostructures hold together and maintain their shape- making sure they work properly when interacting with cells grown in the laboratory or when placed into a living organism.

ABSTRACT

Cell communication which is vital for the proper function, development, and survival of multicellular organisms is often disrupted in diseases. This thesis aims to enhance our understanding of cell communication by employing advanced tools that facilitate the manipulation and analysis of biological systems, spanning from the nanoscale to tissue levels, towards therapeutic applications.

In Paper I, we utilized a microfluidic device to artificially create neuromuscular junctions and gain insights into nerve-muscle communication. We simulated endocrine signaling and the formation of neuromuscular junctions by using myotubes derived from primary mouse myoblasts and motor neurons derived from embryonic stem cells. Transducing skeletal muscle with PGC-1α1, increased the neuromuscular junction formation and size. Neurturin emerged as a mediator in the PGC-1α1-depentent retrograde signaling from muscle to motor neurons. This discovery may pave the way for potential therapies in diseases where neuromuscular junctions are affected early on.

In Paper II, we employed DNA origami nanotechnology to harness the spatial organization of insulin receptors and control multivalent receptor activation. This innovative approach involved assembling insulin into nanoclusters on the surface of DNA origami nanostructures. Beyond in vitro assessments, we extended our investigation to in vivo studies, utilizing a zebrafish model of diabetes. Our findings not only demonstrate the effectiveness of insulin nanoclusters but also highlight the applicability of DNA origami nanostructures in the field of nanomedicine.

In Paper III, we monitored the biodistribution and clearance dynamics of fluorescently labelled DNA origami nanostructures in live zebrafish embryos. We coupled advanced imaging techniques with single-cell RNA sequencing to gain insight into the interactions of DNA nanostructures with biological systems in vivo. This work serves as a guide for evaluating DNA-origami based nanomedicines in animal models.

In Paper IV, we introduce a new method for monitoring the stability of DNA origami nanostructures by using the proximity ligation assay. We were able to detect the preservation of proximity between selected regions when nanostructures were bound to cultured cells as a validation of nanostructure integrity. This approach holds great potential for applications both in vitro and in vivo.

LIST OF SCIENTIFIC PAPERS

I. Richard Mills*, Hermes Taylor-Weiner*, Jorge C. Correia, Leandro Z. Agudelo, Ilary Allodi, **Christina Kolonelou**, Vicente Martinez-Redondo, Duarte M. S Ferreira, Susanne Nichterwitz, Laura H. Comley, Vanessa Lundin, Eva Hedlund, Jorge L. Ruas, Ana I. Teixeira.
Neurturin is a PGC-1α1-controlled myokine that promotes motor neuron recruitment and neuromuscular junction formation.
Mol. Metab. **7**, 12–22 (2018). doi: 10.1016/j.molmet.2017.11.001

II. Joel Spratt*, José M. Dias*, **Christina Kolonelou**, Georges Kiriako, Enya Engström, Ekaterina Petrova, Christos Karampelias, Igor Cervenka, Natali Papanicolaou, Antonio Lentini, Björn Reinius, Olov Andersson, Elena Ambrosetti, Jorge L. Ruas, Ana I. Teixeira.
Multivalent insulin receptor activation using insulin–DNA origami nanostructures.
Nat. Nanotechnol. (2023). doi:10.1038/s41565-023-01507-y

III. **Christina Kolonelou**, Lars Bräutigam, Steven Edwards, Enya Engström, José M. Dias, Joel Spratt, Christos Karampelias, Stefan Wennmalm, Hjalmar Brismar, Olov Andersson, Ana I. Teixeira.
Biodistribution of DNA-origami nanostructures in live zebrafish embryos with single-cell resolution.
(Manuscript).

IV. **Christina Kolonelou**, Ana I. Teixeira
A proximity ligation assay-based method to analyse the integrity of DNA origami nanostructures.
(Manuscript).

*These authors contributed equally to this work.

CONTENTS

LIST OF ABBREVIATIONS

NMJ	Neuromuscular junction
Ach	Acetylocholine
AchR	Acetylocholine receptor
IGF-1	Insuline-like growth factor 1
Eph	Erythropoietin-producing hepatocellular carcinoma
GPI	Glycosylphospatidylinositol-anchored proteins
IGFR	Insulin-like growth factor 1 receptor
IR	Insulin receptor
FRET	Fluorescence resonance energy transfer
BBB	Blood brain barrier
PET	Positron emission technology
PGC1α	Perixosome-proliferator-activated receptor γ coactivator-1a
PDMS	poly (dimethyl siloxane)
GDNF	glial cell-derived neurotrophic factor
BDNF	brain-derived neurotrophic factor
NRTN	neurturin
K-PEG	oligolysine conjugated to polyethylene glycol
mESC	mouse mebryonic stem cell
EB	embryioid body
RA	retinoic acid
SAG	smoothened agonist
NTR	nitroreductase
MTZ	metronidazole
dpf	days post fertilization
dpi	days post injection
hpi	hours post injection
EGFP	enhanced green fluorescent protein
LSFM	light sheet fluorescence microscopy
CHT	caudal hematopoietic tissue
DA	dorsal aorta

α-BTx	alpha bungarotoxin
GFRα2	GDNF family receptor alpha 2
SPR	Surface plasmon resonance
TR	Texas red
RBC	Red blood cell
PLA	Proximity ligation assay
RCA	Rolling circle apmplification

1 LITERATURE REVIEW

1.1 INTRODUCTION

Multicellular organisms are dependent on the coordination of cellular activities, which rely on cell communication among various cell types and tissues. Cell interactions exploit a variety of molecules, including receptors, ligands, junction proteins, integrins, as well as proteins secreted from the extracellular matrix. Extracellular signals are transduced intracellularly through the cell membrane, involving various forms of signaling, such as paracrine, endocrine, synaptic, and contact-dependent. Recipient cells initiate downstream signaling via specific receptors, typically leading to modified transcription factor activity and changes in gene expression. The responsiveness of cells to these cues is evident in the activation of mechanisms governing proliferation, migration, differentiation, apoptosis and more.

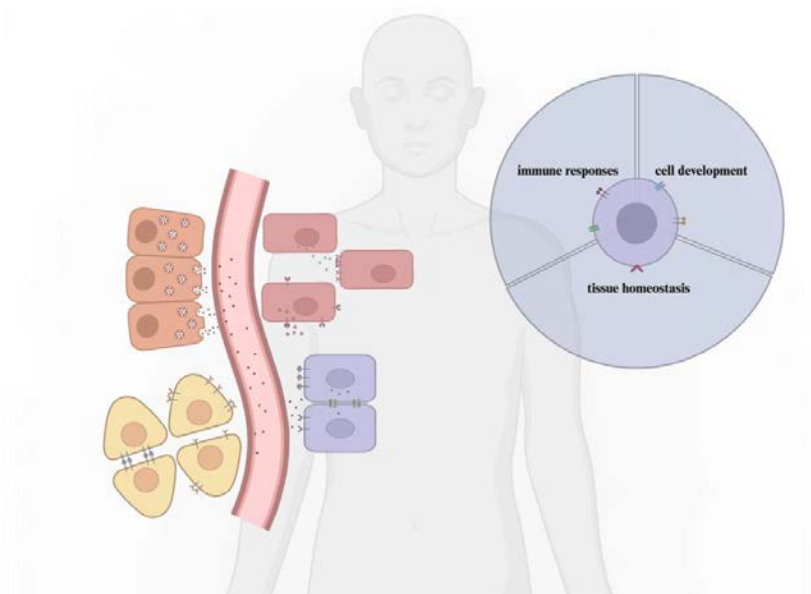

Figure 1. Cell communication in a multicellular organism. Created with BioRender.

At the core of cell communication lies the plasma membrane, serving as the interface that mediates responses to extracellular stimuli and initiates subsequent intracellular biochemical reactions. This intricately structured organelle comprises a continuous lipid bilayer, wherein membrane proteins are embedded and organized into micro- and nanodomains[1,2]. Moreover, membrane protein-cytoskeleton interactions contribute to the dynamic nature of the cell membrane[3]. As a result, signals originating from the microenvironment have the capacity to influence membrane protein organization both temporally and spatially.

Disruptions in cell communication can result in a range of adverse effects, including the development of metabolic and degenerative diseases. Cell communication networks exhibit a high level of complexity, making their study under in vitro conditions technically challenging.

Consequently, the use of tools that provide enhanced cell isolation, precise control over the microenvironment, and the ability to manipulate biological systems spatiotemporally emerges as a viable solution.

1.2 CELL COMMUNICATION AT THE NEUROMUSCULAR JUNCTION

The neuromuscular junction (NMJ) serves as the synapse site where α-motor neurons communicate with myofibers. Signals, in the form of acetylcholine (Ach), are transduced from the nerve (presynaptic part) to the skeletal muscle (postsynaptic part), controlling its function and every voluntary movement. This synaptic connection is formed at the endplate of the sarcolemma of muscle fibers, innervated by a single motor axon in mammals[4].

Components of the NMJ in all vertebrates include the axon terminal, containing vesicles filled with the neurotransmitter Ach, a perisynaptic Schwann cell located at the axon terminal, the synaptic cleft, and the postsynaptic membrane lined with acetylcholine receptors (AchR). Neural impulses trigger the movement of calcium ions into the terminal, leading to Ach release through exocytosis. Ach then binds to AchR, initiating the movement of sodium ions into the muscle cell and simultaneous exit of potassium, resulting in the creation of the endplate potential[5].

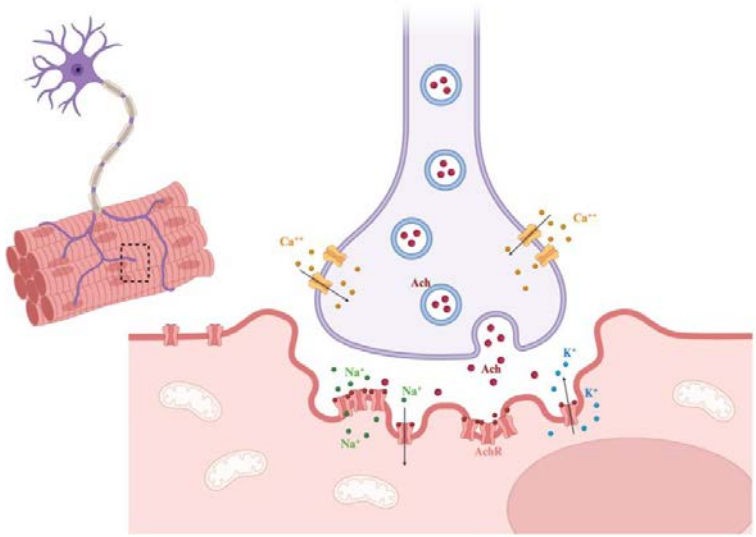

Figure 2. Simplistic illustration of a functional NMJ. Created with BioRender.

The proper development and function of NMJs ensure skeletal muscle function. NMJ dysfunction has been observed in neuromuscular disorders as an early onset symptom.

Studying the microenvironment of NMJ using conventional cell culture approaches poses challenges due to the involvement of different cell types. Microfluidic devices offer a well-

defined system that ensures complete fluidic isolation between compartments, allowing spatially defined control of cellular microenvironments[6]. These devices can be utilized to create in vitro NMJs, where the signals received by motor neurons and muscle fibers can be controlled individually[7,8].

1.3 SPATIAL SIGNALING IN CELL COMMUNICATION

To comprehend the role of individual cells within their local community, it is important to identify the signals exchanged among cells. Assessing the expressed messenger molecules and their associated pathways is essential for elucidating the biological relevance, magnitude, and directionality of cell communication.

While it may seem straightforward, cell-signaling pathways are intricately governed by sophisticated mechanisms. These mechanisms ensure precise, specific, and robust signal transduction to target cells. An example includes post-translational modifications of membrane receptors and their signaling partners, occurring upon ligand binding, which can regulate downstream signal amplification and diversification[9]. Another layer of complexity arises from the tendency of membrane receptors to form multimeric assemblies, influencing their function. A well-studied example of a membrane-bound ligand- receptor pair is that of erythropoietin-producing hepatocellular carcinoma receptors (Eph) and their corresponding ephrin ligands, where receptor activation occurs only after the formation of a tetramer composed of two ephrin ligands and two Eph receptors. This assembly can further lead to the creation of higher-order Eph clusters[10,11].

Taking the above into account, it becomes evident that receptor-mediated signal transduction relies on intricate mechanisms, finely tuned in time and space. Currently, drug development is centered on targeting individual membrane receptors to induce loss of function of their activity. However, this approach may not be desirable when receptors may have multiple functions[12]. Therefore, deciphering the mechanisms of plasma membrane organization could pave the way for more successful strategies in receptor targeting.

The plasma membrane is a dynamic structure that acts not only as a physical barrier between the intracellular and extracellular environment but also as a central hub for numerous biological processes. It consists of various lipids and proteins, which can form complexes and domains of various sizes at different time points. Consequently, the compartmentalization of the plasma membrane results from interactions such as lipid-lipid, protein-lipid, protein-protein, and actin-cytoskeletal interactions[13].

Based on super-resolution microscopy data, membrane proteins can be organized in transient and dynamic assemblies known as nanoclusters. These protein complexes are located at specific membrane regions, often enriched in cholesterol and sphingolipids[14]. Actin cytoskeleton separates these compartments, forming a “picket fence”-like architecture, with the cortical actin cytoskeleton as the fence and transmembrane proteins as the pickets. These proteins, whether lipid-anchored or localized within the membrane, can freely diffuse within

each segmented area. However, the cytoskeleton barrier may prevent them from crossing into another membrane compartment[14]. These nano-sized compartments may serve as physical scaffolds for membrane receptors and their ligands, allowing the formation of clusters. Ultimately, these assemblies can regulate signal transduction through perturbation of their conformation, which propagates across their neighbor binder molecules.

It has been suggested that nanoclustering is a prevalent characteristic of membrane proteins. Examples that provide evidence for nanoclustering on the cell membrane include glycosylphospatidylinositol-anchored proteins (GPI), Ras proteins, T cell receptors, B cell receptor and Eph receptor[9,10,15–17]. Nevertheless, the mechanisms leading to the formation of clusters, their precise size and composition, as well as their multiple functions, remain to be explored.

Deciphering this additional layer of signaling regulation can provide us with the knowledge necessary to overcome challenges in developing strategies for treating diseases. For instance, diabetes and insulin resistance can serve as examples where novel approaches in receptor targeting can be applied. Cross-talk between insulin-like growth factor 1 receptor (IGF-1R) and insulin receptor (IR) can lead to several complications in patients treated for diabetes with insulin injections[18,19]. IRs form clusters in the plasma membrane of β-cells, approximately 60-80 nm in diameter, and their oligomerization state regulates IR signaling[20,21]. The nanoscale organization of IR at the cell membrane could be exploited in a way where multimeric variants of insulin possibly exhibit higher binding affinity to IR than monomeric insulin. This approach could allow for the use of lower concentrations of insulin, thereby decreasing the likelihood of binding to IGF-1R.

Taken together, current therapeutic approaches focusing on individual receptor targeting have limitations and could benefit from refinement. The spatial organization of receptors on the cell membrane creates a complex signaling network, where each molecule seems to exert a distinct effect on signal transduction. Therefore, it is essential to develop tools that enable the characterization and control of membrane protein microenvironments.

1.4 DNA ORIGAMI NANOTECHNOLOGY

The significance of the lateral distribution of membrane proteins for modulating intercellular signaling is widely acknowledged but poorly understood, given challenges in controlling and analyzing membrane protein environments at the nanoscale. Various strategies have been developed to investigate the role of spatial organization of receptors and ligands. These approaches, such as nanolithography and surface-coating methods, primary involve creating ligand nanopatterns on artificially created lipid bilayers to control the spatial organization of ligand-bound receptors at the cell membrane[22,23]. Another approach is to create patterns of ligands on lipid bilayers with the help of metal grids, which prevent lateral mobility and induce clustering of ligands[23]. However, these techniques often fail to precisely control the number of ligands in each nanocluster and their positions relative to one another. Additionally, these

methods rely on surfaces used as substrates for cell culture, limiting their application in physiological environments.

DNA origami nanotechnology is a powerful tool for tailoring the spatial distribution of membrane protein assemblies[24]. It employs DNA self-assembly to construct sophisticated 2D and 3D nanostructures. First introduced by Paul Rothemud in 2006, the technique involved combining a long single stranded DNA molecule (scaffold) with hundreds of short oligonucleotides (staples) in a folding reaction. The yielded product is a folded DNA scaffold of desired shape and dimensions[25]. After Rothemund's exploration of 2D sheets of monolayered DNA helices, the technique was swiftly evolved to fabricate 3D structures of diverse forms, including curved structures, boxes with adjustable lids, and monolithic constructs[25–28]. The production of the early generation of 3D structures was based on densely packing bundles of DNA double-helices in honeycomb or square lattices[25,27,29,30]. Nevertheless, the strategy of densely packing DNA helices involves increased demand on scaffold material, imposing restrictions on the dimensions of structures that can be built. Furthermore, it requires high cationic strength conditions to counteract electrostatic repulsion between the closely packed helices and avoid structural compromise. To address these challenges, novel approaches relying on wireframe designs have been developed for the construction of intricate 2D and 3D polyhedral nanostructures[31–35]. The utilization of sparse wireframe geometries maximizes scaffold length, leading to increased surface areas. Moreover, these nanostructures can be produced while maintaining stability under physiological salt conditions[31], rendering them well-suited for biomedical applications.

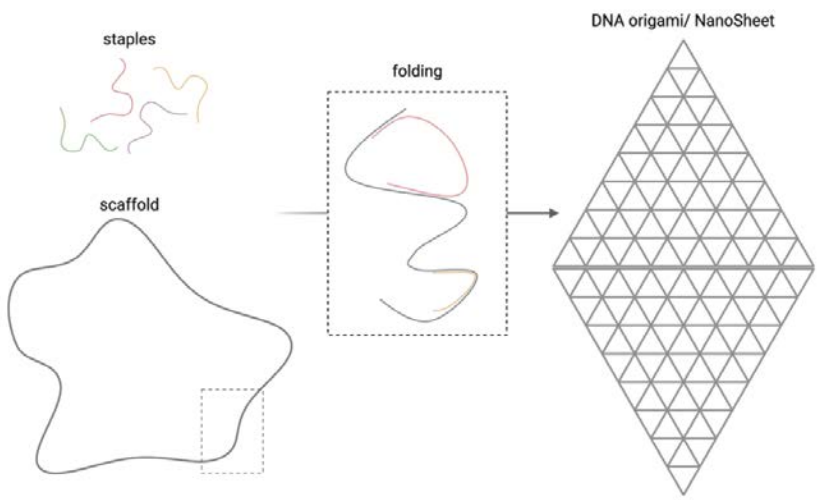

Figure 3. DNA origami technique. Created with BioRender.

1.4.1 Biomedical applications of DNA origami nanostructures

In DNA origami nanostructures the positions of each staple on the scaffold are uniquely and precisely designed. Selecting specific staples for extension with protruding DNA sequences creates sites available for hybridization with complementary oligonucleotides conjugated to biomolecules of interest, such as quantum dots[36], RNA[37], and proteins[38–40]. In this way, DNA nanostructures can serve as scaffolds for assembling various nanoscale biomolecule patterns, exhibiting varying distances and configurations in a robust and efficient manner. Moreover, due to the programmable nature of the protruding sequences, different numbers of functional biomolecules can be displayed on one DNA nanostructure, each placed at a precisely defined location relative to its neighbors[41]. This enables independent variation of the overall spatial organization of biomolecules, irrespective of their total concentration. Consequently, DNA nanostructures have been employed for studying the nanoscale organization of membrane proteins by controlling the spatial distribution of ligands and modulating receptor-mediated signaling in T-cell[42,43], B-cell[44], Eph[24,45], and PD-1[46,47]receptors. In addition, the DNA origami method has been instrumental in constructing nano-rulers for quantitatively assessing super-resolution imaging methods[48–50] and for investigating distance-dependent biomolecular interactions and enzymatic cascades[39,51–53].

In recent years notable advancements have been made in the field of DNA nanotechnology, particularly aimed at facilitating in vivo applications and functioning as versatile therapeutic agents. Due to their inherent biocompatibility and biodegradability, DNA origami nanostructures prove suitable for studies in animal models. To actively target tissues like the immune system and tumors, DNA origami nanostructures have been modified with various biomolecules, including aptamers, antibodies, or other bioactive ligands[54–58]. In contrast, studies have reported the accumulation of unmodified DNA nanostructures in the kidney of mice, suggesting their potential as therapeutic agents capable of mitigating kidney damage[59,60].

1.4.2 DNA origami nanostructures and biological barriers

Despite their potential, DNA origami nanostructures face various challenges when introduced in physiological conditions that must be addressed. These challenges include stability concerns, poor cellular uptake, immune responses, unclear clearance dynamics and biodistribution profiles.

The structural integrity of denser DNA origami nanostructure designs depends on the presence of tens of millimoles of Mg^{2+}, essential to neutralize the electrostatic repulsion between the negatively charged DNA double helices. Various studies have examined the structural integrity of DNA nanostructures in cell culture media, where the Mg^{2+} concentrations were significantly lower than 10mM required in folding reactions[61–63]. These studies indicate that both size and shape play crucial roles in maintaining the stability of low ionic strength. Notably, wireframe technology produces nanostructures of any desired shape under physiological conditions[31], facilitating their applicability for in vivo studies.

The susceptibility of DNA nanostructures to DNA-degrading enzymes has been assessed in vitro using cell lysates, blood serum, or in the presence of high concentrations of DNases[29,61,64]. Varied levels of degradation have been observed in these studies, suggesting that the design of DNA nanostructures plays an important role in determining their vulnerability to DNA degrading enzymes[65,66]. Nevertheless, several strategies have been employed to enhance the overall durability of DNA nanostructures in vitro and in vivo, involving minor groove binders[67], lipid encapsulation[68], polymers[69–71], proteins[72], intercalators like doxorubicin[73], peptoids[74], and PEGylation[75]. The stability of DNA nanostructures has been assessed in vitro through fluorescence resonance energy transfer (FRET)[59,69]. However, it is important to note that this approach is not applicable for in vivo evaluations.

At the cellular level, both the cell membrane and non-functionalized DNA nanostructures are negatively charged, which may lead to lower internalization levels. Nevertheless, studies indicate that more rigid and larger structures demonstrate enhanced internalization efficiency[76,77]. Additionally, different cell types play a pivotal role in the cellular internalization and passive accumulation of DNA nanostructures[59,78]. Therefore, factors such as geometry, design, and cell type collectively influence cellular uptake.

The evaluation of cellular uptake and subcellular localization of DNA origami has been carried out in vitro through fluorescent labeling[76,77,79]. However, this approach presents its own set of challenges. It can be inconclusive concerning the structural integrity of the DNA nanostructures[80–82], and is sensitive to various environmental factors affecting fluorescent dyes[81,83–86].

In vivo, DNA origami nanostructures might encounter another significant biological barrier-the immune system. Studies have documented inflammatory cytokine responses to DNA nanostructures[68,87]. However, it has been demonstrated that employing coating strategies can effectively mitigate these immune responses[68]. Conversely, some studies have observed no immune responses, even in the absence of coating strategies[55,59,88,89]. Despite these findings, drawing definitive conclusions remains challenging. Not all in vivo studies report testing the immunogenic properties of DNA origami nanostructures. Moreover, there are considerable variations in nanostructure designs from one study to another. This variability further complicates our ability to establish conclusive insights into the interaction between DNA origami nanostructures and the immune system.

Developing therapeutic agents with DNA origami nanotechnology requires a precise understanding of the interaction profiles between nanostructures and cells at the whole-body level. Additionally, evaluating the clearance dynamics of DNA nanostructures intravenously injected into a living organism is crucial. While there have been studies performed on mice, assessing the biodistribution profiles of DNA nanostructures[55,59,69,78,89], it is important to note that imaging data acquired with positron emission technology (PET) and bioluminescence pose challenges in terms of resolution and sensitivity.

1.5 ZEBRAFISH AS AN IN VIVO TOOL FOR NANOMEDICINE

Zebrafish (Danio rerio) stands out as a valuable vertebrate model, sharing 70% of the same genes with humans, and showcasing an 82% correspondence of genes related to human diseases[90]. The well-documented organ systems of zebrafish exhibit remarkable physiological homologies with their mammalian counterparts[91,92]. Notable examples include the vasculature system[93–95], blood composition[96,97], lymphatic system[98–101], blood-brain barrier (BBB)[102–104], and liver[105,106]. These characteristics make zebrafish a powerful tool for elucidating the mechanisms underlying human diseases such as diabetes, cancer, and neurodegenerative disorders and for the development of novel therapeutic tools.

Zebrafish embryos and larvae possess advantageous features that make them particularly appealing for studying the functional properties of nanomedicines in vivo. With a high fertilization rate yielding hundreds of embryos weekly and a rapid embryonic development, a significant sample size can be achieved in a short period[92]. Notably, zebrafish embryos undergo swift development, forming complete organ systems including eyes, otic vesicles and the brain within 24 hours post-fertilization[91,107]. The heart[108], and vasculature[109] are fully developed by 48 hours post-fertilization. By 72 hours post-fertilization, the zebrafish pancreas contains a single primary islet[110], and the BBB reaches functional maturity by 5 days post-fertilization[111].

Zebrafish have immune cells akin to those in mammalian immune systems, including neutrophiles[112], macrophages[113], eosinophils[114], natural killer[115], T [116]and B cells[117]. A temporal separation between the activation of innate and adaptive immunity exists, with innate immunity predominating during the first week of development and adaptive immunity being activated later, at three weeks post fertilization[118,119]. This temporal gap is advantageous for investigating interactions of DNA origami nanostructures with the immune system.

Additionally, external fertilization and development in zebrafish allow for direct observation and manipulation. The optical transparency of embryos and larvae, coupled with fluorescent reporter lines (Figure 4) and advanced imaging techniques facilitates high-resolution imaging and tracking of fluorescently labeled objects interacting with biological systems in real-time throughout the entire living organism[120,121]. This combination of features positions zebrafish as a powerful model for dynamic and comprehensive studies in the field.

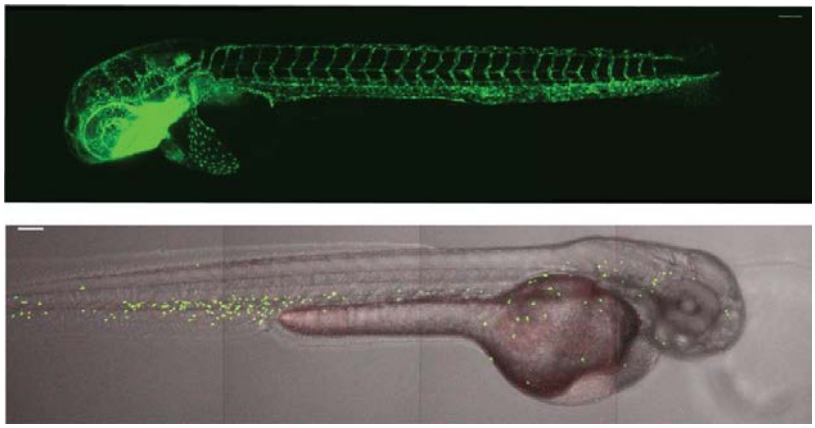

Figure 4. Examples of fluorescent reporter zebrafish lines. Top: A 2 dpf transgenic *Tg(fli1: EGFP)* embryo, with the vasculature shown in green Bottom: A 2 dpf *Tg(mpx:EGFP)* embryo with neutrophils shown in green. Scale bar: 100 μm.

2 RESEARCH AIMS

The aim of the work presented in this thesis is to enhance our understanding of cell communication mechanisms in various biological systems and contribute to the development of novel therapeutic applications. This is achieved by utilizing a broad range of tools and technologies. The following papers specifically aimed:

Paper I. To examine whether overexpression of PGC-1α1 or PGC-1α4 can influence myokine secretion and the formation of NMJ.

Paper II. To investigate the role of insulin valency and spatial organization on IR signaling both in vitro and in vivo, by using insulin- DNA origami nanostructures.

Paper III. To map the biodistribution of DNA origami nanostructures in live zebrafish embryos.

Paper IV. To develop a new method to monitor the stability of DNA origami nanostructures.

3 MATERIAL AND METHODS

3.1 MICROFLUIDIC DEVICE SETUP

In **Paper I**, microfluidic devices fabricated with poly (dimethyl siloxane) (PDMS) served as a platform for developing an in vitro NMJ model[122]. The devices featured two culture compartments, separated by a 150µm microgroove barrier, facilitating communication between them (Figure 5a). Control of the compartment communication is accomplished by creating a difference in hydrostatic pressure between them. When there is a higher volume of medium in one of the compartments, then a small fluid flow towards the opposite compartments is created, counteracting diffusion[122]. This process results in the establishment of fluidic isolation, defining distinct microenvironments within the two compartments.

Myoblasts were seeded first in one compartment, followed by the addition of motor neurons in the adjacent compartment. The differentiation of myoblast into multinucleated muscle fibers extended beyond 48 hours, while the motor neurons remained fluidically isolated. The initiation of axonal recruitment of motor neuron to the muscle compartment was facilitated by a chemotactic gradient of neurotrophic factors. The maturation of the NMJs continued for a duration of 48 hours (Figure 5b).

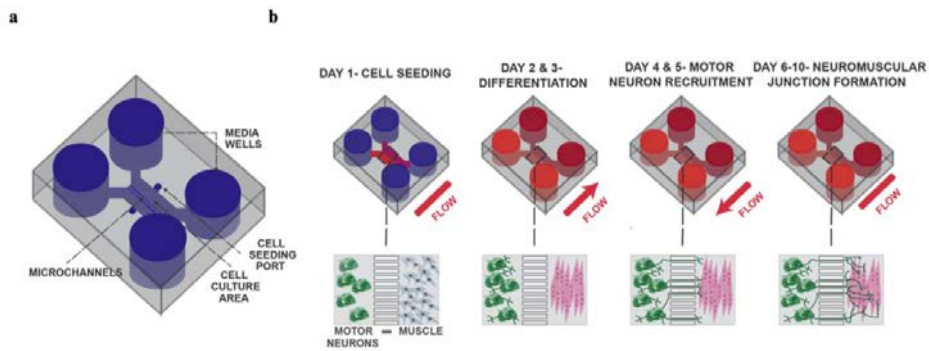

Figure 5. In vitro NMJ set up. **(a)** Schematic representation of the microfluidic device. **(b)** Mouse embryonic stem cell-derived motor neurons and primary myoblasts were seeded in separate compartments through the corresponding seeding port. Myoblasts were differentiated into myofibers for a duration of 48 hours, while motor neurons were kept in fluidic isolation. In days 4 and 5 motor neuron axons were recruited to the muscle side via a chemotactic gradient of glial cell-derived (GDNF) and brain-derived (BDNF) neurotrophic factors (change of the flow direction). The maturation of the formed NMJ took place from day 6 to day 10 under static conditions.

3.2 PRODUCTION OF DNA ORIGAMI NANOSTRUCTURES

In papers II, III, and IV, DNA origami nanostructure designs from previous publications were utilized[24,34]. In Paper II, a rod-shape 18-helix DNA origami design was selected referred to as a NanoRod (Figure 6a,b).

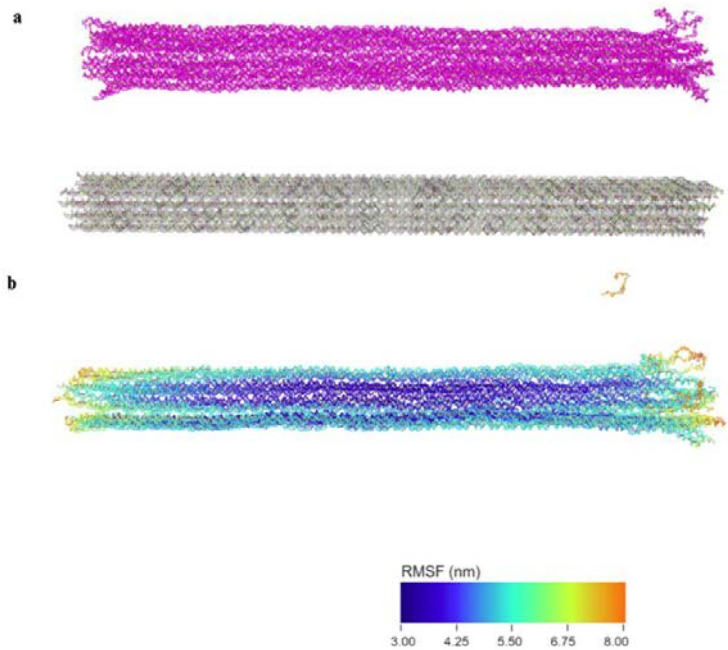

Figure 6. DNA origami NanoRod. **(a)** A schematic illustration of the Nanorod design (grey) and a simulation snapshot of NanoRod structure (pink) generated by the oxDNA software. **(b)** Analysis of the rigidity of NanoRod with the ox DNA coarse-grained modelling software showing a stable solid core with some fluctuations at the ends. RMSF: root mean square fluctuation.

In Papers III and IV, the wireframe DNA origami design was employed to produce single layer two-dimensional sheets, described as NanoSheets (Figure 7a,b). For both designs, scaffold plasmid DNA (p7560 and p8064 respectively) was mixed with a large molar excess of the appropriate staple strands in a "one-pot" folding reaction. The folding buffer for the NanoRod consisted of Tris-acetate-EDTA (TAE, pH 8) and 12.5 mM magnesium chloride ($MgCl_2$). NanoSheets were folded in 1× phosphate-buffered saline (PBS, pH 7.4). The folding reaction of DNA origami nanostructures took place on a thermocycler through an annealing process, which involved an initial heat denaturation step and subsequent gradual cooling over a 14-hour period. The excess of staples was removed from the folded DNA origami nanostructures via diafiltration using Amicon Ultra centrifugal filter columns.

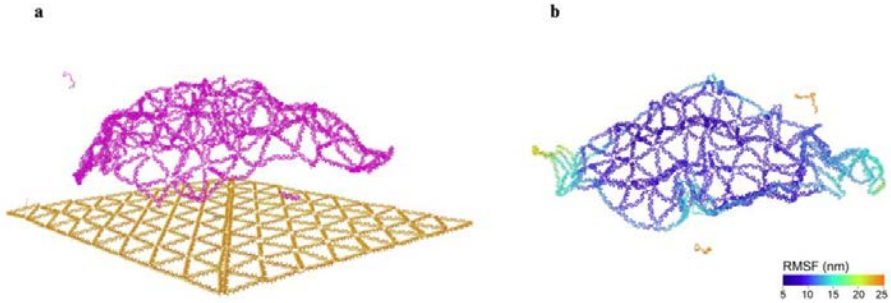

Figure 7. DNA origami NanoSheet. **(a)** An illustration of the NanoSheet design (yellow) compared to a simulation snapshot (pink) of the Nanosheet structure generated by the oxDNA software. (**b)** Rigidity analysis of the NanoSheet, showing a flexible structure. RMSF: root mean square fluctuation.

DNA origami nanostructure designs were modified depending on the aim of each study. Site-specific decoration of DNA origami nanostructures was achieved by incorporating in the staple mix protruding staples containing a 5' overhang sequence on which complementary oligonucleotide sequences, conjugated to molecules of interest, would hybridize.

For both Papers II and III, we employed a coating strategy to enhance nanostructure stability and bioavailability. In this approach, positively charged oligolysine conjugated to polyethylene glycol (K-PEG) electrostatically interacts with the negatively charged DNA nanostructures. To produce the coated nanostructures, NR and NS were mixed with K_{10}-PEG_{5K} at a 1:1 ratio between the amines of lysines in K_{10}-PEG_{5K} and the phosphates in DNA.
The quality of the folded and coated NanoSheet structures was assessed by agarose gel electrophoresis. The neutral surface charge of the coated NS was confirmed by their retention in the well. Treatment of NS with the negatively charged sulfated glycosaminoglycan chondroitin sulfate in 400x excess to the number of amines was used to confirm that nanostructures were not structurally compromised by the coating. Successful removal of the K-PEG coating was confirmed by agarose gel electrophoresis.

3.3 MOUSE EMBRYONIC STEM CELL DIFFERENTIATION

Mouse embryonic stem cells (mESC) expressing GFP under a motor neuron-specific promoter (Eb9) were differentiated into spinal motor neurons using an embryoid body (EB) protocol[123,124]. Briefly, stem cells were expanded for two days, followed by colony dissociation and purification. EB formation was initiated by plating single-cell suspension of stem cells on petri dishes under shaking-culture conditions. Two days later medium was supplemented with with retinoic acid (RA) and the smoothened agonist SAG. On day seven, EBs were dissociated into a single-cell suspension and seeded in the microfluidic devices.

3.4 ZEBRAFISH EMBRYOS EXPERIMENTS

3.4.1 Paper II: Zebrafish β-cell ablation, microinjections, and free glucose quantification

The nitroreductase (NTR)-metronidazole (MTZ) approach[125,126] was employed to induce β-cell loss in zebrafish larvae, creating a diabetes model. Here, a transgenic zebrafish line expressed the bacterial enzyme NTR under the control of the insulin promoter. Treatment with the prodrug MTZ (10mM) resulted in the conversion of MTZ to a toxic byproduct by NTR, specifically and efficiently ablating β-cells.

To assess the ablation protocol in our system, the double-transgenic line *Tg(ins:CFP-NTR);Tg(ins:Kaede)* was used, where the insulin promoter controls the expression of the fluorescent protein Kaede, enabling the visualization of β-cells.

Larvae from the *Tg(ins:CFP-NTR)* line, with ablated β-cells, were intravenously injected with insulin or DNA origami nanostructures at 3 days post-fertilization (dpf). Free glucose levels were measured 4 hours post-injections (hpi) using a fluorescence-based enzymatic kit (BioVision)[127] for glucose measurement.

Microinjections were performed with a pulled glass capillary needle. Larvae were anesthetized at 3dpf, and DNA origami nanostructures were injected into the blood circulation via the common cardinal vein.

3.4.2 Paper III: Transgenic fluorescent zebrafish lines and microinjections

We used the zebrafish model *Tg(fli1:EGFP),* where the expression of green fluorescent protein (EGFP) is under the control of the endothelial specific *fli1* promoter, to visualize the vasculature of the embryo. Additionally, the *Tg(mpeg1:gal4);Tg(UAS:NTR-mCherry)* transgenic line was utilized for conditional targeted macrophage ablation. The macrophage-specific gene marker *mpeg1* allowed for macrophage visualization. Macrophage ablation was induced by MTZ diluted in 1% DMSO in an E3 medium supplemented with 30 mg/ml 1-phenyl-2-thiourea (PTU (10 mM), from 1 dpf and until 72 hpi.

Microinjections were performed with a pulled glass capillary needle. Embryos were anesthetized at 2 dpf, and DNA origami nanostructures were injected into the blood circulation via the common cardinal vein.

3.5 IN VIVO IMAGING EXPERIMENTS

In Paper III, light-sheet fluorescence microscopy (LSFM) imaging was performed with a Light Sheet Z.1 microscope on live NanoSheet-injected *Tg(fli1: EGFP)* embryos at 48 hpf. The embryos were anesthetized and mounted in a low melting point agarose in a glass capillary. During image acquisition, the agarose cylinder containing the embryo was immersed in egg water solution (E3) and the sample chamber temperature was at 28.5°C. Samples were illuminated from two sides and tiled (1 x 3). Z-stacks were acquired every 4 minutes for 4 hours.

For in vivo Airyscan imaging injected embryos were anesthetized and mounted laterally in low melting point agarose on a cover-glass bottomed petri-dish. After agarose polymerization, the dish was filled with egg water solution (E3). The zebrafish caudal hematopoietic tissue (CHT) was imaged on a Zeiss LSM980 Airyscan, with images acquired in the Airscan SR-4Y mode. Fluorescence correlation spectroscopy (FCS) measurements were performed on a Zeiss 980 confocal laser scanning microscope equipped for FCS.
In vivo confocal imaging was performed on live injected embryos and larvae. Anesthetized zebrafish were mounted in methylcellulose and confocal images of their CHT were acquired with a Leica TCS SP8 microscope.

3.6 SINGLE-CELL RNA SEQUENCING EXPERIMENTS

In Paper III, zebrafish embryos injected at 2dpf were dissociated into a single-cell suspension. Four hours post injections, around 200 *Tg(fli1:EGFP)* embryos were euthanized, and tissue dissociation was performed in a "dissociation mix" consisting of trypsin-EDTA and collagenase. Dead cells were stained with DAPI. Texas Red^{+} cells were then FACS sorted on a FACSARIA III with BD FACSDIVA software v. 9.0.1. Viable cells were initially identified by gating cells on FSC-A versus SSC-A, followed by gating on FSC-A versus FSC-H to detect singlets. Then live cells were identified by gating cells on DAPI versus SSC-A. We identified GFP^{+} cells (endothelial cells) by gating FITC-A versus SSC-A. Finally, we gated PE versus FITC-A to detect Texas Red^{+} cells in comparison to the GFP^{+} and GFP^{-} populations. Single-cell RNA sequencing libraries were prepared from the sorted cells using the 10X Genomics Chromium Single Cell 3′ Reagent Kit and sequenced using NextSeq 500/550 High Output Kit on NextSeq 550 platform by Illumina.

3.7 ORIGAMI-PLA

3.7.1 Origami-PLA on a glass surface

Glass coverslips (20mm × 20mm) were cleaned with acetone and isopropanol. Working surfaces were created on the coverslips with the help of Secure Seals and treated first with biotinylated BSA and then with streptavidin, both diluted in buffer containing 10 mM Tris-HCl, 100 mM NaCl, 0.05% and Tween 20. Glass surfaces were exposed to NS decorated with four biotin molecules for 2 min. NS were diluted in buffer containing 5 mM Tris-HCl, 10 mM $MgCl_2$, 1 mM EDTA, and 0.05% Tween 20. Rolling-circle amplification (RCA) reactions took place as described before[128,129]. RCA products were imaged with a Zeiss Axio Imager M2 microscope.

3.7.2 Origami-PLA on MCF7 cells

MCF7 cells were seeded on 13mm cover glasses in 24 well plates. Biotin labeling of the cells was performed with a Sulfo-NHS-LC-Biotin (ThermoFisher Scientific) reagent per manufacturer's instructions. Cells were then fixed in 10% formalin, followed by streptavidin

treatment. NS were immobilized on the cell membrane through biotin-streptavidin interactions and RCA reactions took place[128,129]. Cells were then stained with DAPI and phalloidin 647.

3.8 ETHICAL CONSIDERATIONS

3.8.1 Paper I

The paper consists of in vitro experiments using an established mouse embryonic stem cell line and primary mouse myoblasts. The primary mouse myoblasts were isolated under permit nr. N23/15 issued by Stockholms Norra Djurförsöksetiska nämnd.

3.8.2 Papers II and III

All experiments were performed on animals younger than 5 days and no ethical permit was required according to 2010/63/EU.

4 RESULTS AND DISCUSSION

4.1 PAPER I

4.1.1 Development of a NMJ model in vitro

We established a functional in vitro NMJ model using a microfluid system that grants us full control over the microenvironments of both motor neuron and myotubes (Figure 8). We used a mESC line, where the expression of GFP is under the control of a motor neuron specific promoter[123,124]. By visualizing motor neurons, we were able to assess the differentiation process. Motor neuron progenitors began to express GFP around 24 hours after patterning with retinoic acid (RA) and the smoothened agonist SAG. The differentiation protocol used in this study generates both lateral column and medial motor column motor neurons[130]. We promoted motor neuron recruitment to the muscle compartment with the help of the neurotrophic factors BDNF and GDNF and the presence of NMJ was confirmed by staining with α-bungarotoxin (α-BTX). The function of NMJs was confirmed by myotube contraction induced by motor neuron stimulation with potassium chloride (KCl) and NMJ inhibition using tubocurarine, which is an antagonist of the AChRs.

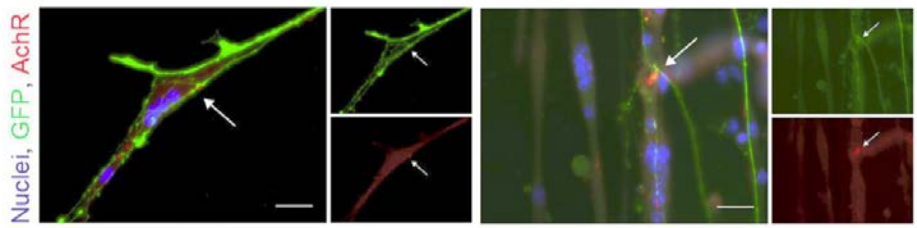

Figure 8. Immunostaining showing the colocalization of Hb9-GFP motor neurons (green), cell nuclei of multinucleated myotubes (blue) and the AchR stain α-BTX (red).

4.1.2 Effect of muscle PGC-1α1 and PGC-1α4 expression levels on in vitro NMJ

Perixosome-proliferator-activated receptor γ coactivator-1alpha (PGC-1α) is essential in regulating of mitochondrial function and energy metabolism, especially in skeletal muscle[131]. Encoded by the PGC-1α gene, there are different splice variants, among which the canonical PGC-1α1 has been identified as a regulator of NMJ structure and activity[132,133]. These variants have been shown to govern oxidative metabolism[134,135]. Notably, the effect of the PGC-1α4 variant on cellular bioenergetic processes is indirect; it induces the expression of insulin-like growth factor 1 (IGF-1) and supresses myostatin, leading to muscle hypertrophy and enhanced strength[136]. Additionally, alterations in PGC-1α1 expression in muscle fibers have been associated with the transformation of motor neurons to a slow phenotype, suggesting the existence of PGC-1α1-dependent retrograde signaling from muscle to motor neurons[137].

To further investigate the roles of PGC-1α1 and PGC-1α4 in retrograde signaling from muscle to motor neurons and their impact on the NMJ, we modified our in vitro system to have

myotubes overexpress PGC-1α1 or PGC-1α4. Leveraging the fluidic isolation provided by the microfluidic devices, we successfully transduced only the myotubes. We observed that only PGC-1α1 expression increased both the formation and size of NMJs. This was shown by the co-localization of AchR and neurofilament. Additionally, AchR clustering was determined by size and staining intensity quantification of AchR aggregates, revealing that overexpression of PGC-1α4 led to smaller clusters. Conversely, the overexpression of PGC-1α1 resulted in an increase in AChR staining intensity.

4.1.3 Microfluidic NMJ model allows for identification of neurturin as a key retrograde factor

The fluidic isolation in the microfluidic devices enabled the analysis of the myokine secretion within the muscle compartment. PGC-1α1 overexpression in myotubes led to an increase of the secretion levels of NRTN. To affirm the responsiveness of motor neurons in our in vitro system to NRTN, we measured the expression levels of the NTRN receptor, GDNF family receptor α2 (GFRα2), during EB formation, and observed a significant increase by day 5. In addition, silencing of NTRN gene expression resulted in inhibiting the enhanced neurite recruitment observed with PGC-1α1 overexpression in muscle. This indicates that NTRN mediates the signaling from muscle to motor neurons under the control of of PGC-1α1. Lastly, we successfully correlated the NTRN expression with PGC-1α1 levels in vivo. NRTN expression levels were quantified with qRT-PCR, showing a significant increase in a mouse model overexpressing PGC-1α1 in skeletal muscle and a significant decrease in a muscle-specific PGC-1α1 KO mouse.

4.2 PAPER II

4.2.1 Control of IR activation by multivalent insulin-NanoRods in vitro

It has been previously reported that IRs form clusters at the plasma membrane of hepatocytes[138], β-cells[139], and adipocytes[140,141]. We confirmed that IRs are organized into nanoclusters at the cell membrane of adipocytes by DNA point accumulation in nanoscale topography (DNA-PAINT)[142]. The average diameter of the clusters was estimated at 74 nm, with three to four IR present per cluster. Notably, this organization was largely maintained after cells were treated with insulin.

Next, we produced NanoRods functionalized with different numbers of insulin peptides, one to fifteen molecules, attached at a range of spacings (Figure 9a,b). The binding kinetics of insulin-NanoRods was determined by surface plasmon resonance (SPR). We observed that nanostructures with multiple insulins showed higher insulin residence time than the monomeric insulin. More importantly, the NanoRod with seven insulin molecules and around 15 nm spacing stood out, showing a substantial decrease of the kinetic dissociation rate (K_{off}) compared to the other designs. This indicates that the binding of insulin-Nanorods to IRs is controlled by insulin valency.

Together with the SPR experiments, we also tested whether the insulin valency affects IR activation at the cell membrane of adipocytes. To achieve this, the phosphorylation levels of IR and the downstream protein AKT were analyzed by western blot. We confirmed that the design of the NanoRods with the seven insulin molecules was also the most effective at activating the IR pathway. In addition, by moving the seven insulins closer together on the NanoRods we observed a decreased IR and AKT phosphorylation. Together, these results show that both insulin spatial configuration and valency control IR activation. Furthermore, RNA sequencing experiments on adipocytes revealed stronger transcriptional responses to multivalent insulin presentation at lower concentrations compared to monomeric insulin.

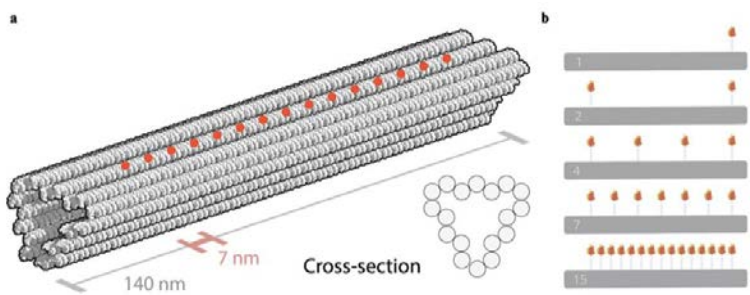

Figure 9. Insulin NanoRods **(a)** The DNA origami NanoRod schematic representation includes red circles denoting the potential positions of protruding staples utilized for the hybridization of complementary oligonucleotides conjugated to insulin. (**b)** Series of NanoRod structures with one to fifteen insulin molecules attached.

4.2.2 Functional effects of multivalent insulin-NanoRods on a zebrafish diabetes model

We further evaluated the performance of nanorods in vivo, using a zebrafish diabetes model. Initially, we investigated the impact of β-cell ablation at 3dpf in *Tg(ins:CFP-NTR);Tg(ins:Kaede)* larvae on their free glucose levels. Notably, we observed an increase in glucose levels compared to animals with non-ablated β-cells. The successful ablation of β-cells was confirmed by quantifying Kaede^{+} cells in *Tg(ins:CFP-NTR);Tg(ins:Kaede)* larvae, showing a significant decrease in cell numbers.

To determine the optimal time frame for observing a reduction in free glucose levels following the β-cell ablation, we injected larvae at 3dpf with insulin and measured free glucose levels at 0.5, 1, and 4 hpi. A consistent normalization was observed at 4 hpi, prompting the selection of this time point for further analysis.

To study the effects of multivalent delivery of insulin in vivo, NanoRods with seven insulin molecules were compared to monovalent insulin NanoRods. To enhance their stability and bioavailability in physiological conditions a K-PEG coating strategy was employed. SPR confirmed the binding of coated NanoRods to IRs, without detecting unspecific binding. Furthermore, the relationship between phosphorylation levels of coated multivalent (NR-7^{KPEG}) and monovalent (NR-1^{KPEG}) NanoRods was maintained, as verified by western blot.

Zebrafish larvae with ablated β-cells were injected with NR-7^{KPEG}, and NR-1^{KPEG}, while non-functionalized (NR^{KPEG}) NanoRods was used as a control condition. Notably, the presence of nanostructures in zebrafish larvae did not significantly affect the numbers of Kaede^{+}cells. Free glucose levels were quantified 4 hpi (Figure 10), showing that larvae treated with NR-7^{KPEG} exhibited significantly decreased free glucose levels compared to those treated with NR^{KPEG}. In contrast, NR-1^{KPEG} did not have a significant effect. Together, these results show that multivalent insulin presentation via NanoRod origami structures successfully stimulates glucose uptake, while structures with only a single insulin molecule fail to elicit a response. This highlights the applicability of DNA origami nanorods in complex biological systems.

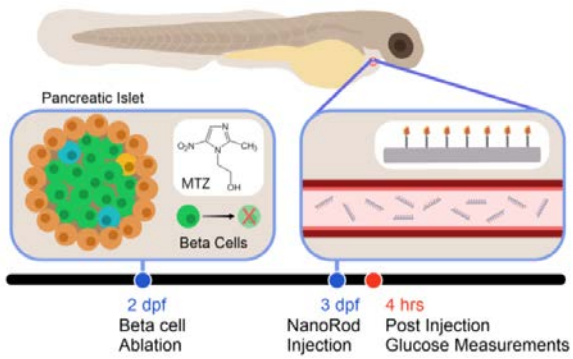

Figure 10. Illustration outlining the approach employed to measure free glucose in zebrafish larvae. β-cell ablation in *Tg(ins:CFP-NTR)* embryos started at 2dpf and lasted for 24 hours.

At 3dpf, larvae were intravenously injected with insulin-NanoRods and four hours later free glucose levels were measured.

4.3 PAPER III

4.3.1 Systemically administrated NanoSheet structures accumulated in the CHT of zebrafish embryos

While DNA origami nanostructures show great promise as multifunctional therapeutic agents, the challenge of accurately assessing their interaction profiles with cells at the whole-body level, as well as understanding their clearance dynamics, persist. Given the zebrafish embryo's emergence as a promising in vivo model in nanomedicine, we selected it as our model system to study the biodistribution profiles of wireframe NanoSheet DNA origami.

NS were fluorescently labeled with Texas Red (TR) and coated with K-PEG (Figure 11). Before injecting them into the blood circulation of 2dpf zebrafish embryos, we investigated whether the coating induced aggregation of NanoSheets in PBS, using Fluorescence Correlation Spectroscopy (FCS). We observed similar diffusion times for fluorescently labeled NanoSheet (NS^{TR}) and NS^{TR} coated with K-PEG ($NS^{TR/K\text{-}PEG}$), indicating that our coating strategy did not result in aggregation of the nanostructures in vitro.

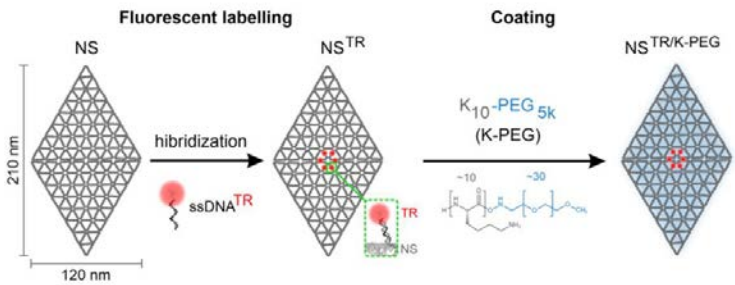

Figure 11. Strategy of fluorescent labeling and coating of NanoSheet, using Texas Red and K_{10}-PEG_{5K} respectively.

We intravenously injected NanoSheets zebrafish embryos at 2 dpf. Shortly after injections, at 0.25 hpi, we performed live whole body LSFM imaging on *Tg(fli1:EGFP)* embryos. At early time points, the fluorescent signal of $NS^{TR/K\text{-}PEG}$ at the CHT was lower than that of NS^{TR}, and it was also detected outside the vasculature. By 4 hpi, both NS^{TR} and $NS^{TR/K\text{-}PEG}$ had accumulated in the CHT of the embryos (Figure 12a). In addition, at 4hpi, the $NS^{TR/K\text{-}PEG}$ signal was detected in other tissues of the embryo, including the brain and muscles. Together these results show the significant role of CHT in the biodistribution of both NS^{TR} and $NS^{TR/K\text{-}PEG}$, with $NS^{TR/K\text{-}PEG}$ showing a different biodistribution profile at the whole animal level when compared to NS^{TR} at early time points.

4.3.2 Dynamics of NanoSheet origami nanostructures clearance at the CHT

We investigated the clearance dynamics of NanoSheets at the CHT by quantifying the fluorescent signal of CHT-resident nanostructures over time. We performed confocal imaging on the CHT of live injected embryos from 4 hpi up to 3 dpi. During this period, the fluorescent intensity of both NS^{TR} and $NS^{TR/K\text{-}PEG}$ decreased. However, only the signal from NS^{TR} decreased down to the control levels at 24h, while the $NS^{TR/KPEG}$ signal was still detectable at 72 hpi. This contrast in clearance dynamics suggest that the K-PEG coating provided prolonged protection to the NS nanostructures accumulated at the CHT.

We further investigated the clearance dynamics at the cellular level by in vivo Airyscan imaging. The CHT of live injected *Tg(fli1:EGFP)* embryos was imaged from 0.5 hpi to 1.5 hpi, when the detected fluorescent signal profiles of NS^{TR} and $NS^{TR/KPEG}$ were significantly different. We observed that NS^{TR} accumulated and degraded faster than $NS^{TR/K\text{-}PEG}$ in cells expressing EGFP. We detected signal only from the $NS^{TR/KPEG}$ structures in $EGFP^{-}$ regions, suggesting their interaction with other than endothelial cells. Furthermore, $NS^{TR/K\text{-}PEG}$ were consistently detected in the bloodstream throughout the experiment, while NS^{TR} were undetectable by 1.5 hpi. Notably, $NS^{TR/K\text{-}PEG}$, but not NS^{TR}, were detected in the bloodstream long after the microinjections.

To investigate whether the K-PEG coated NanoSheets aggregate in the circulation before accumulating in cells at the CHT, we performed FCS in the lumen of the dorsal aorta (DA) of the embryos (Figure 12b). Analysis of the $NS^{TR/KPEG}$ brightness revealed that they started to aggregate in circulation at 2 hpi, with the size of aggregates increasing over time. This indicated that the aggregation process did not impact the observed clearance dynamics of the coated NanoSheets at earlier time points. These results indicate that the endothelial cells at the CHT are the primary cell type interacting with the NS nanostructures. Nevertheless, the K-PEG coating affected the clearance profiles of NanoSheets, with only $NS^{TR/K\text{-}PEG}$ demonstrating interaction with CHT cells other than the endothelial cells.

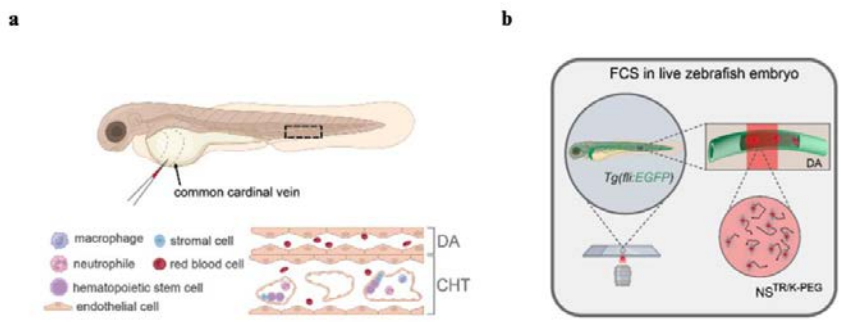

Figure 12. **(a)** Illustration showing the site of microinjections at 2 dpf embryos. Boxed region showing the cell types found in the DA and CHT of zebrafish embryos. **(b)** Overview of the *in vivo* FCS experiment.

4.3.3 A single-cell resolution profiling of NanoSheet-interacting cells in zebrafish embryos

We performed whole embryo transcriptome analysis of NanoSheet-interacting cells and identified ten different cell types for both NS^{TR} and $NS^{TR/KPEG}$ injected embryos (Figure 13). Notably, vascular/scavenger endothelial cells constituted 45.39% of the total NS^{TR}-interacting population, in contrast to a mere 14.03% in $NS^{TR/KPEG}$-interacting cells. Mesenchymal neural crest cells, comprising 30% of the total population, constituted the largest group among $NS^{TR/K-PEG}$- interacting cells. Additionally, the percentages of cells identified as embryonic brain, red blood cells (RBC), the musculature system and muscle cells were higher in $NS^{TR/K-PEG}$- than NS^{TR}-interacting cells. At the 4hpi time point, the percentage of immune cells was low in both unoated and coated NS; however, it was more than two-fold higher in $NS^{TR/K-PEG}$- than in NS^{TR}-interacting cells. Together, these results suggest that coating with K-PEG facilitates a broader distribution of NanoSheet nanostructures throughout the entire zebrafish embryo, enabling their interaction with tissues beyond the CHT.

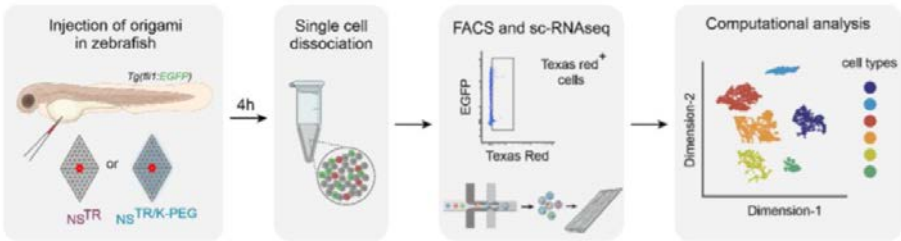

Figure 13. General overview of the strategy to identify cells interacting with NanoSheet structures.

4.3.4 Contribution of CHT-resident macrophages to NanoSheet clearance

The results of our whole-body single-cell transcriptome analysis of zebrafish embryos at 4 hpi suggested that a limited number of macrophages, identified by the expression of the macrophage-specific gene marker *mpeg1*, interacted with the NS nanostructures. Subsequently, we further investigated the role of CHT-resident macrophages to the clearance dynamics at later time points (Figure 14). We observed that the detected signal from the NS without the K-PEG coating was significantly higher in macrophage-ablated embryos compared to macrophage-non-ablated embryos, at 48 hpi and 72 hpi. Conversely, the ablation of macrophages did not significantly affect the signal from the $NS^{TR/K-PEG}$ at these time points. This indicates that the macrophages that reside at the CHT begin to contribute in the clearance of the NS^{TR} days after the injection of the nanostructures into the embryos' bloodstream. Additionally, the results suggest that our coating strategy protects against clearance by macrophages within the CHT.

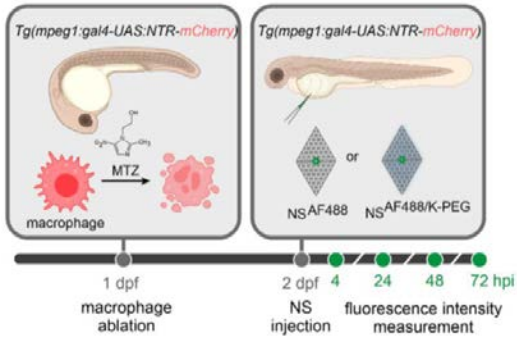

Figure 14. The role of CHT-resident macrophages in NS clearance was evaluated using the strategy outlined here.

4.4 PAPER IV

4.4.1 Origami-PLA method development

The structural integrity of DNA origami nanostructures in complex biological systems remains a challenge yet to be addressed. This project focuses on the development of a novel method for monitoring the stability of DNA origami nanostructures both in vitro and in vivo.

Our approach is based on proximity ligation assay (PLA) and depends on the proximity between two protruding DNA strands (PLA protruding strands) on the surface of NanoSheet structures. These strands serve as starting points for rolling cycle amplification (RCA) reactions, which can be detected by fluorescently labeled oligonucleotides[128]. The lack of a fluorescent signal suggests that the DNA nanostructures are structurally compromised.

We modified NS nanostructures with two sets of a pair of DNA protruding strands, designed to be positioned at a nominal distance of 30 nm between the two pairs (NS_PLA). Hybridization with two complementary connector oligonucleotides followed by enzymatic DNA ligation, leads to the formation of a circular DNA molecule, which acts as a template for RCA reactions. The resulting RCA product can then be detected by fluorescently labeled oligonucleotides binding to complementary sequences present on the RCA product (Figure 15). Therefore, the absence of a fluorescent signal indicates that the DNA nanostructures are structurally compromised.

To confirm that the acquired signal is generated due to the proximity of the protruding strands of the same NanoSheet, we used a mixture of nanostructures with only one of the protruding sequences present at their surface as a negative control (NS_green and NS_blue).

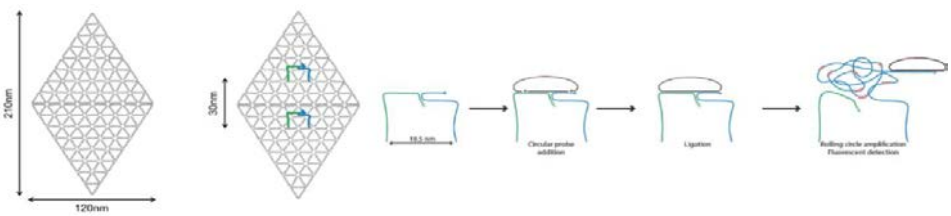

Figure 15. Schematic outline of the method. ssDNA protruding strands positioned at the surface of DNA origami nanostructures can serve as a template for rolling cycle amplification reactions. Wireframe NanoSheet origami nanostructures were modified with two sets of a pair of DNA protruding strands that were positioned at a 30 nm distance between the two pairs (NS_PLA). The distance between the two DNA protruding strands in each pair is 18.5 nm. The proximity of the two protruding DNA strands allows the complementary hybridization of two connector oligonucleotides, which can form a circular molecule by enzymatic DNA ligation. After ligation, RCA reactions can take place and the amplification product can be detected by fluorescently labeled oligonucleotides, which bind to complementary sites of the RCA product.

Using agarose gel electrophoresis, we observed consistent migration patterns among NS_PLA, NS_green, and NS_blue structures. We designed two sets of oligonucleotides complementary to the PLA ssDNA protruding strands, with biotin conjugated to their 3' end. These were used to confirm the positions of the two sets of the PLA protruding strands through biotin-streptavidin using AFM.

The method's development began with an in vitro validation. DNA nanostructures were immobilized on a glass surface via biotin-streptavidin interactions. NS nanostructures with two pairs of protruding DNA sequences placed on proximity (18.5nm) were tested, successfully generating a clear PLA signal. Notably, the signal acquired from the control condition was lower compared to the NS_PLA.

We further tested the method on a highly complex biological surface- the cellular membrane. We biotinylated the cell membrane proteins of MCF7 cells and through biotin-streptavidin binding we immobilized NS_PLA nanostructures on their surface. The generated PLA signal from NS_PLA structures was significantly higher compared to the negative control.

To evaluate the structural integrity of the NanoSheets, we exposed them for 24 h to different concentrations of DNaseI, confirming degradation with agarose gel electrophoresis. Notably, quantification of NanoSheet band intensities showed that the nanostructures were already structurally compromised at a relatively low DNaseI concentration of 2U/ml.

Additionally, DNA nanostructures were coated with a protective PEGylated oligolysine shell (K-PEG)[69] to test its ability to slow down nuclease degradation and preserve their structural integrity. After removing the K-PEG coating with chondroitin sulfate treatment we assessed the structural integrity of the structures with agarose gel electrophoresis. Quantification of the bands showed that coated structures preserved their structural integrity.

5 CONCLUSIONS

This thesis presents a highly interdisciplinary body of work integrating microfluidics, cell biology techniques, DNA origami nanotechnology, advanced imaging methods, next-generation sequencing, and animal experiments to study mechanisms of cell communication from nanoscale to tissue level.

In Paper I, we used a microfluidic co-culture device to enable precise directional control of communication between motor neurons and muscle. This model allowed us to individually control the microenvironmental cues received by these two cell types. Not only did this setup facilitate the generation of a functional NMJ, but also it provided a means to control the direction of paracrine signaling. Our findings confirmed that PGC-1α1 expression in skeletal muscle regulates NMJ structure and activity, as evidenced by increased neuronal recruitment and larger NMJs in our system, Significantly, we identified neurturin as a muscle-derived soluble factor controlled by PGC-1α1, mediating retrograde signaling to motor neurons.

In Paper II, we used DNA origami nanotechnology as a precision tool to generate ligand clusters at the nanometer level. This approach allowed us to control receptor activation and achieve a tunable signaling response in cells. Specifically, our work using insulin-DNA origami nanostructures demonstrated that the valency and spacing of insulin molecules can be engineered to result in prolonged periods of receptor activation compared to monomeric insulin. Additionally, the multivalent insulin not only inactivated the same downstream transcriptional responses as monomeric insulin but also achieved these effects at lower concentrations. Of particular significance, when treating a zebrafish embryo model of diabetes with rising glucose levels, multivalent insulin nanostructures elicited the desired response of glucose reduction, while monomeric insulin at the same concentration failed to do so. The knowledge gained from this study provides a basis for development of novel therapeutic approaches in diabetes treatment, offering the potential to achieve desirable outcomes without relying on higher doses of insulin.

DNA origami nanostructures hold great promise as versatile therapeutic agents. However, realizing their full potential involves navigating certain challenges. In Paper III, we presented a strategy that facilitated the assessment of DNA origami nanostructures' biodistribution within a living organism and with single cell resolution. This innovative approach combined DNA nanotechnology with embryonic zebrafish models, advanced microscopy, and single-cell RNA sequencing. Our study identified scavenger endothelial cells as the primary contributors to the clearance dynamics of NanoSheet origami structures in our system, while macrophages became involved in the process at later time points. This work offers a guide for assessing the in vivo performance of DNA origami nanostructures, a critical step in advancing potential therapeutic applications in the future.

In Paper IV, we introduced a method for monitoring the stability of DNA origami nanostructures under physiological conditions. Our work demonstrated the effectiveness of this

method in detecting the structural integrity of DNA origami nanostructures when immobilized on both glass surfaces and cell membranes. This work presents a promising approach for assessing the structural integrity of DNA origami nanostructures in vitro as well as in vivo.

6 POINTS OF PERSPECTIVE

In Paper I, we used a microfluidic system to achieve enhanced control over the microenvironment of motor neurons and myotubes. Through this approach we identified NRTN as a myokine involved in retrograde signaling to motor neurons. To delve deeper into understanding its role in the communication between motor neurons and muscle, exploring the modulation of NRTN expression in muscle holds the potential to yield valuable insights into its biological activities. This, in turn, could pave the way for exploring its therapeutic applications in neuromuscular disorders.

In Paper II, we employed DNA origami nanotechnology and showed that the manipulation of insulin nanoclusters' valency and geometry provides control over IR-mediated responses. A study on IR clusters in different cell types, coupled with an in-depth investigation of the biodistribution profiles of multivalent insulin-DNA origami designs in both wild type and diabetes animal models, such as zebrafish embryos, would be of a great interest. This approach, offering single-cell resolution analyses, is essential for advancing our understanding of how to precisely target individual tissues and effectively eliminate unwanted interactions. Further testing the effects of multivalent insulin-DNA origami nanostructures in mice, a more clinically relevant model, could bring us closer to the development of new drugs for the treatment of diabetes.

Paper III introduces an approach to assess the biodistribution and clearance dynamics of DNA origami nanostructures in a complex biological system with single-cell resolution. A study where DNA origami nanostructures are selectively directed towards specific tissues, via functionalization with ligands of interest, could provide additional insights into their properties and further demonstrate the sensitivity of our approach. Additionally, validating the utility of our approach by comparing the performances of multiple origami designs in the same sample would be of great interest.

In Paper IV, we present a PLA-based method to assess the structural integrity of DNA origami nanostructures. It would be of great interest to further test the method on nanostructures of various shapes and sizes. Moreover, the approach shows great promise for applications in in vivo models, especially in tracking the stability of DNA origami nanostructures in different tissues- a goal that should be pursued.

7 ACKNOWLEDGEMENTS

During my PhD journey, I had the pleasure to work with several great scientists from many fields of research.

Ana, my main supervisor, thank you for giving me the opportunity to perform my doctoral research in your group. Your support on unique and interdisciplinary projects, together with your ability to envision the big picture, has been inspiring. A big thank you to my co-supervisors, Björn, Ernest, and Olov.

I am truly grateful to my collaborators who have played a pivotal role in my research work. **Lars**, thank you for listening to my ideas and answering my questions throughout these years. Your scientific guidance, the generous sharing of knowledge, the help and discussions have been invaluable. **Steve**, thank you for always being so kind, helpful and for teaching me so many things about LSFM. **Olov**, besides being an excellent collaborator, your role as my co-supervisor has been instrumental. **Christo**, your support in my zebrafish experiments has been truly appreciated. **Stefan,** thank you for our nice collaboration and introducing me to FCS.
A special thank you to past and present Teixeira group members and collaborators; **Hermes**, **Siji**, **Alessandro**, and **Elena** thank you for having such a positive energy and always being so helpful. **Joel** thank you for being a fantastic collaborator and a great colleague. **Georges** and **José**, thank you for always being friendly and helpful. **Enya**, our teamwork has been excellent, and our friendly chats are always appreciated.
To all the wonderful people at **B9 quarter** for creating a pleasant working atmosphere, a big thank you.

To my friends- **Julia** thank you for being a true friend and a great flatmate. Thank you for the great chats and for always being there, through good and bad times. **Mary**, your friendship, the fun and relaxing moments, and all the craziness have been a true joy. **Niko**, **Anastasia** and **Valia**- thank you for the cherished memories from our Uppsala days to the present.
Muyi, **Pedro**, **Mathilde and Lia**, your fantastic company, laughter, and culinary delights have been a highlight.
A big thank you to friends from back home and everyone who crossed my path over those years, for being by my side and enjoying life's moments together.

My biggest thank you to those who have always been part of my life. **Μαμά**, **μπαμπά**, **Σταυρούλα** σας ευχαριστώ πολύ για την στήριξη, την εμπιστοσύνη και την αγάπη σας όλα αυτά τα χρόνια.

Finally, my sweetest thank you to the most important people in my life; To my **Sander**, thank you for your endless support, unconditional love and for always being on my side.
To my **Ianthe**, thank you for our great adventures together, your unconditional love and for inspiring me to be the best version of myself.

8 REFERENCES

1. Geiger, B., Spatz, J. P. & Bershadsky, A. D. Environmental sensing through focal adhesions. *Nat. Rev. Mol. Cell Biol.* **10**, 21–33 (2009).

2. Sezgin, E., Levental, I., Mayor, S. & Eggeling, C. The mystery of membrane organization: composition, regulation and roles of lipid rafts. *Nat. Rev. Mol. Cell Biol.* **18**, 361–374 (2017).

3. Kosmalska, A. J. *et al.* Physical principles of membrane remodelling during cell mechanoadaptation. *Nat. Commun.* **6**, 7292 (2015).

4. Wilson, M. H. & Deschenes, M. R. The neuromuscular junction: Anatomical features and adaptations to various forms of increased, or decreased neuromuscular activity. *Int. J. Neurosci.* **115**, 803–828 (2005).

5. Wood, S. J. & R. Slater, C. Safety factor at the neuromuscular junction. *Prog. Neurobiol.* **64**, 393–429 (2001).

6. K. Young, E. W. & J. Beebe, D. Fundamentals of microfluidic cell culture in controlled microenvironments. *Chem. Soc. Rev.* **39**, 1036–1048 (2010).

7. Deleglise, B. *et al.* Synapto-Protective Drugs Evaluation in Reconstructed Neuronal Network. *PLOS ONE* **8**, e71103 (2013).

8. Deleglise, B. *et al.* β-amyloid induces a dying-back process and remote trans-synaptic alterations in a microfluidic-based reconstructed neuronal network. *Acta Neuropathol. Commun.* **2**, 145 (2014).

9. Deribe, Y. L., Pawson, T. & Dikic, I. Post-translational modifications in signal integration. *Nat. Struct. Mol. Biol.* **17**, 666–672 (2010).

10. Seiradake, E., Harlos, K., Sutton, G., Aricescu, A. R. & Jones, E. Y. An extracellular steric seeding mechanism for Eph-ephrin signaling platform assembly. *Nat. Struct. Mol. Biol.* **17**, 398–402 (2010).

11. Himanen, J. P. *et al.* Architecture of Eph receptor clusters. *Proc. Natl. Acad. Sci.* **107**, 10860–10865 (2010).

12. Genander, M. *et al.* Dissociation of EphB2 Signaling Pathways Mediating Progenitor Cell Proliferation and Tumor Suppression. *Cell* **139**, 679–692 (2009).

13. Harding, A. S. & Hancock, J. F. Using plasma membrane nanoclusters to build better signaling circuits. *Trends Cell Biol.* **18**, 364–371 (2008).

14. Saka, S. K. *et al.* Multi-protein assemblies underlie the mesoscale organization of the plasma membrane. *Nat. Commun.* **5**, 4509 (2014).

15. Himanen, J. P. *et al.* Architecture of Eph receptor clusters. *Proc. Natl. Acad. Sci.* **107**, 10860–10865 (2010).

16. Shen, K., Thomas, V. K., Dustin, M. L. & Kam, L. C. Micropatterning of costimulatory ligands enhances CD4+ T cell function. *Proc. Natl. Acad. Sci.* **105**, 7791–7796 (2008).

17. Yokosuka, T. *et al.* Spatiotemporal Regulation of T Cell Costimulation by TCR-CD28 Microclusters and Protein Kinase C θ Translocation. *Immunity* **29**, 589–601 (2008).

18. Clayton, P. E., Banerjee, I., Murray, P. G. & Renehan, A. G. Growth hormone, the insulin-like growth factor axis, insulin and cancer risk. *Nat. Rev. Endocrinol.* **7**, 11–24 (2011).

19. Schumacher, R., Mosthaf, L., Schlessinger, J., Brandenburg, D. & Ullrich, A. Insulin and insulin-like growth factor-1 binding specificity is determined by distinct regions of their cognate receptors. *J. Biol. Chem.* **266**, 19288–19295 (1991).

20. Boothe, T. *et al.* Inter-domain tagging implicates caveolin-1 in insulin receptor trafficking and Erk signaling bias in pancreatic beta-cells. *Mol. Metab.* **5**, 366–378 (2016).

21. Kubar, J. & Van Obberghen, E. Oligomeric states of the insulin receptor: binding and autophosphorylation properties. *Biochemistry* **28**, 1086–1093 (1989).

22. Yao, X., Peng, R. & Ding, J. Cell–Material Interactions Revealed Via Material Techniques of Surface Patterning. *Adv. Mater.* **25**, 5257–5286 (2013).

23. Salaita, K. *et al.* Restriction of Receptor Movement Alters Cellular Response: Physical Force Sensing by EphA2. *Science* **327**, 1380–1385 (2010).

24. Shaw, A. *et al.* Spatial control of membrane receptor function using ligand nanocalipers. *Nat. Methods* **11**, 841–846 (2014).

25. Rothemund, P. W. K. Folding DNA to create nanoscale shapes and patterns. *Nature* **440**, 297–302 (2006).

26. Andersen, E. S. *et al.* Self-assembly of a nanoscale DNA box with a controllable lid. *Nature* **459**, 73–76 (2009).

27. Douglas, S. M. *et al.* Self-assembly of DNA into nanoscale three-dimensional shapes. *Nature* **459**, 414–418 (2009).

28. Han, D. *et al.* DNA Origami with Complex Curvatures in Three-Dimensional Space. *Science* **332**, 342–346 (2011).

29. Castro, C. E. *et al.* A primer to scaffolded DNA origami. *Nat. Methods* **8**, 221–229 (2011).

30. Ke, Y. *et al.* Multilayer DNA Origami Packed on a Square Lattice. *J. Am. Chem. Soc.* **131**, 15903–15908 (2009).

31. Benson, E. *et al.* DNA rendering of polyhedral meshes at the nanoscale. *Nature* **523**, 441–444 (2015).

32. Zhang, F. *et al.* Complex wireframe DNA origami nanostructures with multi-arm junction vertices. *Nat. Nanotechnol.* **10**, 779–784 (2015).

33. Veneziano, R. *et al.* Designer nanoscale DNA assemblies programmed from the top down. *Science* **352**, 1534–1534 (2016).

34. Benson, E. *et al.* Computer-Aided Production of Scaffolded DNA Nanostructures from Flat Sheet Meshes. *Angew. Chem. Int. Ed.* **55**, 8869–8872 (2016).

35. Jun, H. *et al.* Autonomously designed free-form 2D DNA origami. *Sci. Adv.* **5**, eaav0655 (2019).

36. Bui, H. *et al.* Programmable Periodicity of Quantum Dot Arrays with DNA Origami Nanotubes. *Nano Lett.* **10**, 3367–3372 (2010).

37. Ke, Y., Lindsay, S., Chang, Y., Liu, Y. & Yan, H. Self-Assembled Water-Soluble Nucleic Acid Probe Tiles for Label-Free RNA Hybridization Assays. *Science* **319**, 180–183 (2008).

38. Rinker, S., Ke, Y., Liu, Y., Chhabra, R. & Yan, H. Self-assembled DNA nanostructures for distance-dependent multivalent ligand–protein binding. *Nat. Nanotechnol.* **3**, 418–422 (2008).

39. Voigt, N. V. *et al.* Single-molecule chemical reactions on DNA origami. *Nat. Nanotechnol.* **5**, 200–203 (2010).

40. Derr, N. D. *et al.* Tug-of-War in Motor Protein Ensembles Revealed with a Programmable DNA Origami Scaffold. *Science* **338**, 662–665 (2012).

41. Bila, H., Paloja, K., Caroprese, V., Kononenko, A. & Bastings, M. M. C. Multivalent Pattern Recognition through Control of Nano-Spacing in Low-Valency Super-Selective Materials. *J. Am. Chem. Soc.* **144**, 21576–21586 (2022).

42. Dong, R. *et al.* DNA origami patterning of synthetic T cell receptors reveals spatial control of the sensitivity and kinetics of signal activation. *Proc. Natl. Acad. Sci.* **118**, e2109057118 (2021).

43. Hellmeier, J. *et al.* Strategies for the Site-Specific Decoration of DNA Origami Nanostructures with Functionally Intact Proteins. *ACS Nano* **15**, 15057–15068 (2021).

44. Veneziano, R. *et al.* Role of nanoscale antigen organization on B-cell activation probed using DNA origami. *Nat. Nanotechnol.* **15**, 716–723 (2020).

45. Verheyen, T. *et al.* Spatial organization-dependent EphA2 transcriptional responses revealed by ligand nanocalipers. *Nucleic Acids Res.* **48**, 5777–5787 (2020).

46. Paloja, K. *et al.* Balancing the Nanoscale Organization in Multivalent Materials for Functional Inhibition of the Programmed Death-1 Immune Checkpoint. *ACS Nano* **18**, 1381–1395 (2024).

47. Fang, T. *et al.* Spatial Regulation of T-Cell Signaling by Programmed Death-Ligand 1 on Wireframe DNA Origami Flat Sheets. *ACS Nano* **15**, 3441–3452 (2021).

48. Steinhauer, C., Jungmann, R., Sobey, T. L., Simmel, F. C. & Tinnefeld, P. DNA Origami as a Nanoscopic Ruler for Super-Resolution Microscopy. *Angew. Chem. Int. Ed.* **48**, 8870–8873 (2009).

49. Schmied, J. J. *et al.* DNA origami–based standards for quantitative fluorescence microscopy. *Nat. Protoc.* **9**, 1367–1391 (2014).

50. Raab, M. *et al.* Using DNA origami nanorulers as traceable distance measurement standards and nanoscopic benchmark structures. *Sci. Rep.* **8**, 1780 (2018).

51. Le, J. V. *et al.* Probing Nucleosome Stability with a DNA Origami Nanocaliper. *ACS Nano* **10**, 7073–7084 (2016).

52. Fu, J. *et al.* Assembly of multienzyme complexes on DNA nanostructures. *Nat. Protoc.* **11**, 2243–2273 (2016).

53. Shaw, A. *et al.* Binding to nanopatterned antigens is dominated by the spatial tolerance of antibodies. *Nat. Nanotechnol.* **14**, 184–190 (2019).

54. Wang, Z. *et al.* A Tubular DNA Nanodevice as a siRNA/Chemo-Drug Co-delivery Vehicle for Combined Cancer Therapy. *Angew. Chem. Int. Ed.* **60**, 2594–2598 (2021).

55. Li, S. *et al.* A DNA nanorobot functions as a cancer therapeutic in response to a molecular trigger in vivo. *Nat. Biotechnol.* **36**, 258–264 (2018).

56. Liu, S. *et al.* A DNA nanodevice-based vaccine for cancer immunotherapy. *Nat. Mater.* **20**, 421–430 (2021).

57. Qin, X. *et al.* Tetrahedral framework nucleic acids-based delivery of microRNA-155 inhibits choroidal neovascularization by regulating the polarization of macrophages. *Bioact. Mater.* **14**, 134–144 (2022).

58. Joseph, N. *et al.* Biodistribution and function of coupled polymer-DNA origami nanostructures. *Sci. Rep.* **13**, 19567 (2023).

59. Jiang, D. *et al.* DNA origami nanostructures can exhibit preferential renal uptake and alleviate acute kidney injury. *Nat. Biomed. Eng.* **2**, 865–877 (2018).

60. Chen, Q. *et al.* Sequential Therapy of Acute Kidney Injury with a DNA Nanodevice. *Nano Lett.* **21**, 4394–4402 (2021).

61. Hahn, J., Wickham, S. F. J., Shih, W. M. & Perrault, S. D. Addressing the Instability of DNA Nanostructures in Tissue Culture. *ACS Nano* **8**, 8765–8775 (2014).

62. Kielar, C. *et al.* On the Stability of DNA Origami Nanostructures in Low-Magnesium Buffers. *Angew. Chem. Int. Ed.* **57**, 9470–9474 (2018).

63. Kocabey, S. *et al.* Cellular Uptake of Tile-Assembled DNA Nanotubes. *Nanomaterials* **5**, 47–60 (2015).

64. Mei, Q. *et al.* Stability of DNA Origami Nanoarrays in Cell Lysate. *Nano Lett.* **11**, 1477–1482 (2011).

65. Ramakrishnan, S. *et al.* Real-Time Observation of Superstructure-Dependent DNA Origami Digestion by DNase I Using High-Speed Atomic Force Microscopy. *ChemBioChem* **20**, 2818–2823 (2019).

66. Suma, A., Stopar, A., Nicholson, A. W., Castronovo, M. & Carnevale, V. Global and local mechanical properties control endonuclease reactivity of a DNA origami nanostructure. *Nucleic Acids Res.* **48**, 4672–4680 (2020).

67. Wamhoff, E.-C. *et al.* Controlling Nuclease Degradation of Wireframe DNA Origami with Minor Groove Binders. *ACS Nano* **16**, 8954–8966 (2022).

68. Perrault, S. D. & Shih, W. M. Virus-Inspired Membrane Encapsulation of DNA Nanostructures To Achieve In Vivo Stability. *ACS Nano* **8**, 5132–5140 (2014).

69. Ponnuswamy, N. *et al.* Oligolysine-based coating protects DNA nanostructures from low-salt denaturation and nuclease degradation. *Nat. Commun.* **8**, 15654 (2017).

70. Agarwal, N. P., Matthies, M., Gür, F. N., Osada, K. & Schmidt, T. L. Block Copolymer Micellization as a Protection Strategy for DNA Origami. *Angew. Chem. Int. Ed.* **56**, 5460–5464 (2017).

71. Anastassacos, F. M., Zhao, Z., Zeng, Y. & Shih, W. M. Glutaraldehyde Cross-Linking of Oligolysines Coating DNA Origami Greatly Reduces Susceptibility to Nuclease Degradation. *J. Am. Chem. Soc.* **142**, 3311–3315 (2020).

72. Lacroix, A., Edwardson, T. G. W., Hancock, M. A., Dore, M. D. & Sleiman, H. F. Development of DNA Nanostructures for High-Affinity Binding to Human Serum Albumin. *J. Am. Chem. Soc.* **139**, 7355–7362 (2017).

73. Ijäs, H. *et al.* Unraveling the interaction between doxorubicin and DNA origami nanostructures for customizable chemotherapeutic drug release. *Nucleic Acids Res.* **49**, 3048–3062 (2021).

74. Wang, S.-T. *et al.* DNA origami protection and molecular interfacing through engineered sequence-defined peptoids. *Proc. Natl. Acad. Sci.* **117**, 6339–6348 (2020).

75. Bujold, K. E. *et al.* Sequence-responsive unzipping DNA cubes with tunable cellular uptake profiles. *Chem. Sci.* **5**, 2449–2455 (2014).

76. Wang, P. *et al.* Visualization of the Cellular Uptake and Trafficking of DNA Origami Nanostructures in Cancer Cells. *J. Am. Chem. Soc.* **140**, 2478–2484 (2018).

77. Bastings, M. M. C. *et al.* Modulation of the Cellular Uptake of DNA Origami through Control over Mass and Shape. *Nano Lett.* **18**, 3557–3564 (2018).

78. Zhang, Q. *et al.* DNA Origami as an In Vivo Drug Delivery Vehicle for Cancer Therapy. *ACS Nano* **8**, 6633–6643 (2014).

79. Liang, L. *et al.* Single-Particle Tracking and Modulation of Cell Entry Pathways of a Tetrahedral DNA Nanostructure in Live Cells. *Angew. Chem. Int. Ed.* **53**, 7745–7750 (2014).

80. Green, C. M., Mathur, D. & Medintz, I. L. Understanding the fate of DNA nanostructures inside the cell. *J. Mater. Chem. B* **8**, 6170–6178 (2020).

81. Koga, M. M., Comberlato, A., Rodríguez-Franco, H. J. & Bastings, M. M. C. Strategic Insights into Engineering Parameters Affecting Cell Type-Specific Uptake of DNA-Based Nanomaterials. *Biomacromolecules* **23**, 2586–2594 (2022).

82. Lacroix, A., Vengut-Climent, E., de Rochambeau, D. & Sleiman, H. F. Uptake and Fate of Fluorescently Labeled DNA Nanostructures in Cellular Environments: A Cautionary Tale. *ACS Cent. Sci.* **5**, 882–891 (2019).

83. Chen, A. K., Cheng, Z., Behlke, M. A. & Tsourkas, A. Assessing the Sensitivity of Commercially Available Fluorophores to the Intracellular Environment. *Anal. Chem.* **80**, 7437–7444 (2008).

84. Zheng, Q., Jockusch, S., Zhou, Z. & Blanchard, S. C. The Contribution of Reactive Oxygen Species to the Photobleaching of Organic Fluorophores. *Photochem. Photobiol.* **90**, 448–454 (2014).

85. Kretschy, N., Sack, M. & Somoza, M. M. Sequence-Dependent Fluorescence of Cy3- and Cy5-Labeled Double-Stranded DNA. *Bioconjug. Chem.* **27**, 840–848 (2016).

86. Hedegaard, S. F. *et al.* Fluorophore labeling of a cell-penetrating peptide significantly alters the mode and degree of biomembrane interaction. *Sci. Rep.* **8**, 6327 (2018).

87. Schüller, V. J. *et al.* Cellular Immunostimulation by CpG-Sequence-Coated DNA Origami Structures. *ACS Nano* **5**, 9696–9702 (2011).

88. Xia, K. *et al.* Systematic Study in Mammalian Cells Showing No Adverse Response to Tetrahedral DNA Nanostructure. *ACS Appl. Mater. Interfaces* **10**, 15442–15448 (2018).

89. Wamhoff, E.-C. *et al.* Evaluation of Nonmodified Wireframe DNA Origami for Acute Toxicity and Biodistribution in Mice. *ACS Appl. Bio Mater.* **6**, 1960–1969 (2023).

90. Howe, K. *et al.* The zebrafish reference genome sequence and its relationship to the human genome. *Nature* **496**, 498–503 (2013).

91. Nusslein-Volhard, C. & Dahm, R. *Zebrafish*. (OUP Oxford, 2002).

92. Kimmel, C. B., Ballard, W. W., Kimmel, S. R., Ullmann, B. & Schilling, T. F. Stages of embryonic development of the zebrafish. *Dev. Dyn.* **203**, 253–310 (1995).

93. Isogai, S., Horiguchi, M. & Weinstein, B. M. The Vascular Anatomy of the Developing Zebrafish: An Atlas of Embryonic and Early Larval Development. *Dev. Biol.* **230**, 278–301 (2001).

94. Ellertsdóttir, E. *et al.* Vascular morphogenesis in the zebrafish embryo. *Dev. Biol.* **341**, 56–65 (2010).

95. Herwig, L. *et al.* Distinct Cellular Mechanisms of Blood Vessel Fusion in the Zebrafish Embryo. *Curr. Biol.* **21**, 1942–1948 (2011).

96. Chen, A. T. & Zon, L. I. Zebrafish blood stem cells. *J. Cell. Biochem.* **108**, 35–42 (2009).

97. Thisse, C. & Zon, L. I. Organogenesis--Heart and Blood Formation from the Zebrafish Point of View. *Science* **295**, 457–462 (2002).

98. Koltowska, K. *et al.* Vegfc Regulates Bipotential Precursor Division and Prox1 Expression to Promote Lymphatic Identity in Zebrafish. *Cell Rep.* **13**, 1828–1841 (2015).

99. Hogan, B. M. *et al.* Vegfc/Flt4 signalling is suppressed by Dll4 in developing zebrafish intersegmental arteries. *Development* **136**, 4001–4009 (2009).

100. Küchler, A. M. *et al.* Development of the Zebrafish Lymphatic System Requires Vegfc Signaling. *Curr. Biol.* **16**, 1244–1248 (2006).

101. Koltowska, K., Betterman, K. L., Harvey, N. L. & Hogan, B. M. Getting out and about: the emergence and morphogenesis of the vertebrate lymphatic vasculature. *Development* **140**, 1857–1870 (2013).

102. Li, Y. *et al.* Zebrafish: A promising in vivo model for assessing the delivery of natural products, fluorescence dyes and drugs across the blood-brain barrier. *Pharmacol. Res.* **125**, 246–257 (2017).

103. Kim, S. S. *et al.* Zebrafish as a Screening Model for Testing the Permeability of Blood–Brain Barrier to Small Molecules. *Zebrafish* **14**, 322–330 (2017).

104. Umans, R. A. & Taylor, M. R. Zebrafish as a Model to Study Drug Transporters at the Blood–Brain Barrier. *Clin. Pharmacol. Ther.* **92**, 567–570 (2012).

105. Chu, J. & Sadler, K. C. New school in liver development: Lessons from zebrafish. *Hepatology* **50**, 1656–1663 (2009).

106. Field, H. A., Dong, P. D. S., Beis, D. & Stainier, D. Y. R. Formation of the digestive system in zebrafish. ii. pancreas morphogenesis☆. *Dev. Biol.* **261**, 197–208 (2003).

107. Kari, G., Rodeck, U. & Dicker, A. P. Zebrafish: An Emerging Model System for Human Disease and Drug Discovery. *Clin. Pharmacol. Ther.* **82**, 70–80 (2007).

108. Scott, I. C. & Yelon, D. Chapter 1.4 - Cardiac Development in the Zebrafish. in *Heart Development and Regeneration* (eds. Rosenthal, N. & Harvey, R. P.) 103–120 (Academic Press, Boston, 2010). doi:10.1016/B978-0-12-381332-9.00004-9.

109. Okuda, K. S. & Hogan, B. M. Endothelial Cell Dynamics in Vascular Development: Insights From Live-Imaging in Zebrafish. *Front. Physiol.* **11**, (2020).

110. Karampelias, C. *et al.* Reinforcing one-carbon metabolism via folic acid/Folr1 promotes β-cell differentiation. *Nat. Commun.* **12**, 3362 (2021).

111. O'Brown, N. M. *et al.* The secreted neuronal signal Spock1 promotes blood-brain barrier development. *Dev. Cell* **58**, 1534-1547.e6 (2023).

112. Bennett, C. M. *et al.* Myelopoiesis in the zebrafish, Danio rerio. *Blood* **98**, 643–651 (2001).

113. Herbomel, P., Thisse, B. & Thisse, C. Zebrafish Early Macrophages Colonize Cephalic Mesenchyme and Developing Brain, Retina, and Epidermis through a M-CSF Receptor-Dependent Invasive Process. *Dev. Biol.* **238**, 274–288 (2001).

114. Lieschke, G. J., Oates, A. C., Crowhurst, M. O., Ward, A. C. & Layton, J. E. Morphologic and functional characterization of granulocytes and macrophages in embryonic and adult zebrafish. *Blood* **98**, 3087–3096 (2001).

115. Pereiro, P. *et al.* Zebrafish Nk-lysins: First insights about their cellular and functional diversification. *Dev. Comp. Immunol.* **51**, 148–159 (2015).

116. Trede, N. S. & Zon, L. I. Development of t-cells during fish embryogenesis. *Dev. Comp. Immunol.* **22**, 253–263 (1998).

117. Renshaw, S. A. & Trede, N. S. A model 450 million years in the making: zebrafish and vertebrate immunity. *Dis. Model. Mech.* **5**, 38–47 (2012).

118. Herbomel, Philippe, Thisse, B. & Thisse, C. Ontogeny and behaviour of early macrophages in the zebrafish embryo. *Development* **126**, 3735–3745 (1999).

119. Lam, S. H., Chua, H. L., Gong, Z., Lam, T. J. & Sin, Y. M. Development and maturation of the immune system in zebrafish, Danio rerio: a gene expression profiling, in situ hybridization and immunological study. *Dev. Comp. Immunol.* **28**, 9–28 (2004).

120. Hayashi, Y. *et al.* Differential Nanoparticle Sequestration by Macrophages and Scavenger Endothelial Cells Visualized in Vivo in Real-Time and at Ultrastructural Resolution. *ACS Nano* **14**, 1665–1681 (2020).

121. Arias-Alpizar, G. *et al.* Light-triggered switching of liposome surface charge directs delivery of membrane impermeable payloads in vivo. *Nat. Commun.* **11**, 3638 (2020).

122. Taylor, A. M. *et al.* A microfluidic culture platform for CNS axonal injury, regeneration and transport. *Nat. Methods* **2**, 599–605 (2005).

123. Di Giorgio, F. P., Carrasco, M. A., Siao, M. C., Maniatis, T. & Eggan, K. Non–cell autonomous effect of glia on motor neurons in an embryonic stem cell–based ALS model. *Nat. Neurosci.* **10**, 608–614 (2007).

124. Wichterle, H., Lieberam, I., Porter, J. A. & Jessell, T. M. Directed Differentiation of Embryonic Stem Cells into Motor Neurons. *Cell* **110**, 385–397 (2002).

125. Curado, S. *et al.* Conditional targeted cell ablation in zebrafish: A new tool for regeneration studies. *Dev. Dyn.* **236**, 1025–1035 (2007).

126. Pisharath, H., Rhee, J. M., Swanson, M. A., Leach, S. D. & Parsons, M. J. Targeted ablation of beta cells in the embryonic zebrafish pancreas using E. coli nitroreductase. *Mech. Dev.* **124**, 218–229 (2007).

127. Jurczyk, A. *et al.* Dynamic glucoregulation and mammalian-like responses to metabolic and developmental disruption in zebrafish. *Gen. Comp. Endocrinol.* **170**, 334–345 (2011).

128. Söderberg, O. *et al.* Direct observation of individual endogenous protein complexes in situ by proximity ligation. *Nat. Methods* **3**, 995–1000 (2006).

129. Clausson, C.-M. *et al.* Compaction of rolling circle amplification products increases signal integrity and signal-to-noise ratio. *Sci. Rep.* **5**, 12317 (2015).

130. Allodi, I. & Hedlund, E. Directed midbrain and spinal cord neurogenesis from pluripotent stem cells to model development and disease in a dish. *Front. Neurosci.* **8**, (2014).

131. Lin, J., Handschin, C. & Spiegelman, B. M. Metabolic control through the PGC-1 family of transcription coactivators. *Cell Metab.* **1**, 361–370 (2005).

132. Handschin, C. *et al.* PGC-1α regulates the neuromuscular junction program and ameliorates Duchenne muscular dystrophy. *Genes Dev.* **21**, 770–783 (2007).

133. Arnold, A.-S. *et al.* Morphological and functional remodelling of the neuromuscular junction by skeletal muscle PGC-1α. *Nat. Commun.* **5**, 3569 (2014).

134. Zhang, Y. *et al.* Alternative mRNA Splicing Produces a Novel Biologically Active Short Isoform of PGC-1α*. *J. Biol. Chem.* **284**, 32813–32826 (2009).

135. Miura, S., Kai, Y., Kamei, Y. & Ezaki, O. Isoform-Specific Increases in Murine Skeletal Muscle Peroxisome Proliferator-Activated Receptor-γ Coactivator-1α (PGC-1α) mRNA in Response to β2-Adrenergic Receptor Activation and Exercise. *Endocrinology* **149**, 4527–4533 (2008).

136. Ruas, J. L. *et al.* A PGC-1α Isoform Induced by Resistance Training Regulates Skeletal Muscle Hypertrophy. *Cell* **151**, 1319–1331 (2012).

137. Chakkalakal, J. V., Nishimune, H., Ruas, J. L., Spiegelman, B. M. & Sanes, J. R. Retrograde influence of muscle fibers on their innervation revealed by a novel marker for slow motoneurons. *Development* **137**, 3489–3499 (2010).

138. Li, H. *et al.* Mechanism of INSR clustering with insulin activation and resistance revealed by super-resolution imaging. *Nanoscale* **14**, 7747–7755 (2022).

139. Boothe, T. *et al.* Inter-domain tagging implicates caveolin-1 in insulin receptor trafficking and Erk signaling bias in pancreatic beta-cells. *Mol. Metab.* **5**, 366–378 (2016).

140. Jarett, L. & Smith, R. M. The natural occurrence of insulin receptors in groups on adipocyte plasma membranes as demonstrated with monomeric ferritin-insulin. *J. Supramol. Struct.* **6**, 45–59 (1977).

141. Gustavsson, J. *et al.* Localization of the insulin receptor in caveolae of adipocyte plasma membrane. *FASEB J.* **13**, 1961–1971 (1999).

142. Jungmann, R. *et al.* Multiplexed 3D cellular super-resolution imaging with DNA-PAINT and Exchange-PAINT. *Nat. Methods* **11**, 313–318 (2014).